COATING OF SPINEL LAYERS ON ALUMINA BY ELECTROSTATIC SPRAY DEPOSITION (ESD)

A Thesis Submitted to

the Graduate School of Engineering and Sciences of

İzmir Institute of Technology

in Partial Fulfillment of the Requirements for the Degree of

MASTER OF SCIENCE

in Materials Science and Engineering

by

İrem DEMİRKOL

April, 2023

İZMİR

ACKNOWLEDGEMENTS

First of all, I would like to acknowledge and give my warmest thanks to my supervisor Prof. Dr. Sedat AKKURT for his guidance, advice, motivation, support, trust, and tolerance through all the stages of this thesis and my master degree program of material science and engineering. It is a pleasure and honor to be his student.

Secondly, I would like to thank research assistants, dear Tuğçe ÖZMEN EGESOY and Emre ERĞEN for their help, support and friendship during the laboratory works and through my master degree program.

Finally, I would like to express my sincere thanks to my beloved parents and my sister, Hülya DEMİRKOL and Ufuk DEMİRKOL and Yelda DEMİRKOL for their everlasting love, support, motivation, trust and tolerance throughout my whole life. Endless thanks for always being there for me.

ABSTRACT

COATING OF SPINEL LAYERS ON ALUMINA BY ELECTROSTATIC SPRAY DEPOSITION (ESD)

$MgAl_2O_4$ spinel layer was coated on dense alumina pellets by advantageous ESD among the other deposition methods in terms of providing a simple, inexpensive setup and good control of the layer morphology. The main goals are successfull deposition of spinel layers on alumina pellets by ESD, to investigate the effect of ESD parameters (working distance, flow rate of precursors, applied voltage) on coating microstructure by conducting full factorial design experiments and to determine the best experimental conditions for a porous layer. Besides, $MgCr_2O_4$ layer was coated on dense alumina and $MgAl_2O_4$ layer was deposited on bisque-fired alumina pellet to extend the scope of the work. Alumina powders were compressed and sintered, respectively to obtain pellets. $MgAl_2O_4$ spinel precursor solution was sprayed on the alumina pellets by changing the parameters accordingly the full factorial design. $MgAl_2O_4$ and $MgCr_2O_4$ solutions were also sprayed on the bisque-fired and the dense alumina pellets with the parameters given the best porous layer. Elemental analysis of the residues obtained after evaporation of the solutions by energy dispersive X-ray spectroscopy (EDX), both unheated and post-heated residual powders of solutions by X-ray diffraction (XRD) and surface morphologies of coated pellets by scanning electron microscopy (SEM-EDS) were analyzed. Spinel layers on alumina pellets were successfully coated by ESD, which could provide variable surface morphologies. The optimum conditions for a porous layer were obtained as working distance of 15 mm, flow rate of 0.25 mL/h and applied voltage of 6 kV in this study. The coatings on the pellets before further heating were amorphous. Post-heating of the pellets were required to obtain crystalline spinel structure.

ÖZET

ELEKTROSTATİK SPREY KAPLAMA (ESD) METODU İLE ALÜMİNA ÜZERİNE SPİNEL FİLMLERİN KAPLANMASI

ESD, kullanım kolaylığı, ekonomik düzeneği ve iyi kaplama morfolojisi kontrolü ile diğer kaplama tekniklerinden avantajlı durumdadır. Bu çalışmada $MgAl_2O_4$ spinel yapısı alümina peletler üzerine ESD ile kaplanmıştır. Temel amaçlar, ESD ile alümina üzerine spinel katmanlarını başarılı bir şekilde biriktirmek, tam faktöriyel tasarım deneyleri yaparak ESD parametrelerinin (çalışma mesafesi, öncül çözeltinin püskürtme hızı ve uygulanan voltaj) kaplama mikroyapısı üzerindeki etkilerini incelemek ve gözenekli kaplamayı oluşturan en iyi deneysel koşulları belirlemektir. Ayrıca, alümina pelet üzerine $MgCr_2O_4$ ve bisküvi pişirimli alümina pelet üzerine $MgAl_2O_4$ spinel tabakası kaplanarak çalışmanın kapsamı genişletilmek istenmiştir. Alümina tozu preslenmiş ve fırında sinterlenerek peletler hazırlanmıştır. $MgAl_2O_4$ çözeltisi, peletler üzerine, parametreler tam faktöriyel tasarıma göre değiştirilerek püskürtülmüştür. $MgAl_2O_4$ ve $MgCr_2O_4$ çözeltileri de gözenekli kaplamanın elde edildiği parametrelerle bisküvi ve yoğun peletlere püskürtülmüştür. Çözeltilerin element analizi, enerji dağılımlı X-ışını spektroskopi (EDX) ile, sinterlenmemiş ve sinterlenmiş çözelti tozları X-ışını kırınımı (XRD) ile, kaplamaların morfolojileri, taramalı elektron mikroskobu (SEM-EDS) ile analiz edilmiştir. Alümina peletler spinel yapıyla ESD kullanılarak başarılı bir şekilde kaplanmıştır. ESD ile çok çeşitli yüzey morfolojilerinin elde edilebilir olduğu görülmüştür. Gözenekli bir kaplama için optimum koşullar çalışma mesafesi 15 mm, akış hızı 0,25 mL/h ve voltaj 6 kV olarak elde edilmiştir. Peletler üzerindeki kaplamalar amorf yapılardır ve kristal spinel yapıyı elde etmek için kaplanan peletlerin, kaplama sonrasında ısıl işleme tabi tutulması gerektiği sonucuna varılmıştır.

TABLE OF CONTENTS

LIST OF FIGURES

Figure **Page**

Figure **Page**

Figure **Page**

Figure **Page**

Figure **Page**

LIST OF TABLES

Table **Page**

Table **Page**

CHAPTER 1

INTRODUCTION

Ceramics, one of the main sub-groups of solid materials, are defined as compounds between metallic and non-metallic elements.

Ceramic materials can be grouped into two categories: traditional or classical ceramics and modern or technical ceramics. Cement, glass and those composed of clay minerals can be referred as traditional ceramics, while oxides, nitrides and carbides such as aluminum oxide (or alumina, Al_2O_3), silicon dioxide (or silica, SiO_2), silicon carbide (SiC), silicon nitride (Si_3N_4) are some common examples of modern ceramics.

Ceramic materials are stiff, typically very hard and their strengths are similar to those of the metals. They used to be brittle and highly sensitive to fracture. However, they are able to be engineered to become more resistant to fracture. Besides, they typically have low electrical and thermal conductivities and resistant to high temperatures and severe situations. They can be optically varied: transparent and translucent and/or opaque [1].

Alumina, which is one of the modern ceramic materials, is quite attractive for many engineering applications due to its availability, chemical and thermal stability, its relatively good strength and thermal-electrical insulation [2]. Alumina is widely used in industrial areas such as most of the electrical and mechanical applications, integrated circuits, transistor pads, thin film backing, furnace tube used in corrosive environments, laboratory utensils, cutting tips, nuclear ceramics etc.

Alumina is generally produced by a method called Bayer process. The raw material entering this process is called bauxite. Bauxite consists of a mixture of different aluminum hydrates. It may also contain impurities such as iron oxide, silicate. In Bayer process, Bauxite, powder of 1mm and containing 55-60% Al_2O_3, is processed in sodium solution at 250 °C and pressure of 4 N/mm^2 . The resulting sodium-aluminate solution is filtered and mixed with extra aluminum hydroxide and water and taken into large tanks. It is calcined in rotary kilns at 1200-1300 °C until α-Al_2O_3 is formed. Afterwards, this calcined product is ground. Apart from Bayer method, there are also different production methods of alumina [3]. They are shown in Figure 1.1 [4].

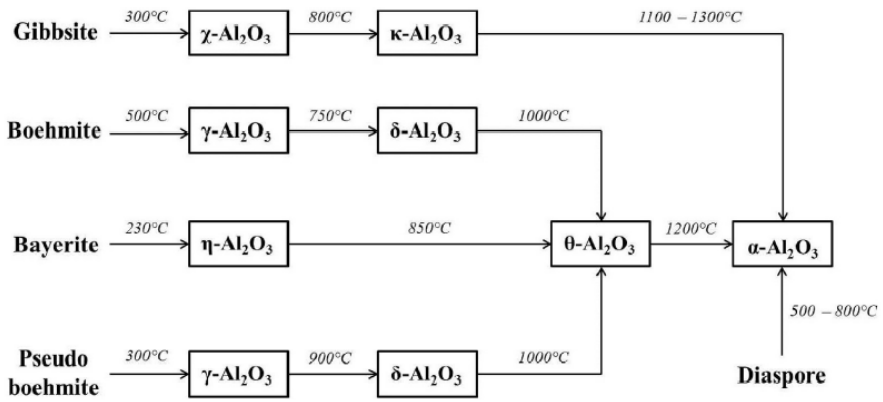

Figure 1.1. Different production methods of alumina by thermal treatment of corresponding aluminum hydroxides [4].

Spinel, one of the other advanced ceramic materials, can be simply defined as a group of minerals consisting of oxides of magnesium, aluminum, iron, manganese, chromium, etc. The spinel structure is formulated as AB_2X_4. A and B are tetrahedrally and octahedrally coordinated cations, and X is an anion which is typically O or F. If X is oxygen, the spinel structure is called oxide spinel whose formula is AB_2O_4. The name spinel comes from the mineral $MgAl_2O_4$ [5].

Magnesium aluminate spinel has got magnificent properties such as high melting point, low thermal conductivity, high corrosion resistance and low thermal expansion [6]. It is usually utilized in optical and refractory applications.

There are several ways to make $MgAl_2O_4$, including sol-gel, self-heat-sustained (SHS), and solid state synthesis [7].

Solid-state reactions are frequently used in synthetic processes to produce polycrystalline materials from solid reagents and they are one of the most common methods to produce $MgAl_2O_4$ spinel. Quite high temperature is needed for the reaction to take place in solid state synthesis. Chemical and morphological properties of the reagents such as the reactivity, surface area, and free energy change with the solid-state reaction, and temperature, pressure and the environment of the reaction affect the reaction. Solid-state reaction method is very useful and common technique due to its ease of process and possibility of high volume of production [8]. In solid state synthesis, methodology can be simply explained as follows: Preparation of the raw materials, calcination of the materials and sintering process.

Due to its excellent optical transparency, thermal stability, chemical inertness, and minimal electrical conductivity, magnesium aluminate ($MgAl_2O_4$) has been undergone extensive research due to its potential as an effective coating [9].

In the literature, there are numerous deposition methods stated which can be chosen in accordance with the material to be deposited, the required coating quality, and the available budget. Some of them can be listed as vacuum deposition techniques like physical vapour deposition, sputtering, pulsed laser deposition chemical vapour deposition, liquid-precursor-based thin film deposition techniques such as spray deposition methods. These spray deposition methods are electrostatic spray deposition, flame spray deposition, ultrasonic spray prolysis, mist spray prolysis. Moreover, electrophoretic deposition, spin and dip coating, sol-gel method are the other techniques [10].

The electrostatic spray deposition, also known as ESD, has many advantages over other deposition techniques, including high deposition efficiency because the droplets are transported by electrical forces rather than a carrier gas as in conventional sprays, a simple and inexpensive setup, a large selection of precursors, good control of the film stoichiometry, because it is the same as that of the precursor solutions, and good morphology control. It is anticipated that the layer and substrate will adhere quite well [11].

ESD is a process in which a precursor solution is atomized by an electric field into an aerosol and then directed toward a heated substrate to deposit a thin coating. This method works effectively to deposit controlled microstructures.

The substrate temperature, nozzle to substrate distance, flow rate of the precursor solution, applied voltage, physical and chemical properties of the precursor solutions (solubility, boiling point, conductivity, surface tension, viscosity, density), and the deposition time all affect the microstructure of the ESD coatings.

Yalamac et al. investigated the microstructure of the interface between co-sintering and co-pressed alumina-spinel compacts and diffusion couples of alumina and spinel. A spinel ($MgO{\cdot}Al_2O_3$) phase occurs in the middle of magnesia (MgO) and alumina (Al_2O_3), when they are heated together. In order to determine if a strong bond may be formed between magnesia (MgO) and alumina (Al_2O_3) or to explore the diffusion behaviors of the constituents, the extent of the creation of the spinel phase or the interface has been researched from various angles. To comprehend the development of intermediate new phases between the two end-members (components) that have already

been somewhat shaped and sintered, diffusion couple testing is a helpful and widely used approach. Figure 1.2 and 1.3 reveal the microstructure of alumina A–spinel bi-materials. At 1500 °C, new columnar spinel grains formed when alumina and spinel were co-sintered. From the original spinel-alumina interface, these columnar spinel grains formed and developed into alumina. All two scenarios are believed to be possible as far as how the columnar spinel grains develop and grow. These are magnesium vapor transport inside the porous spinel component and volume diffusion inside the columnar grains. It was discovered that the co-sintering of two isothermal steps produced columnar spinel grains with two different morphologies. The same columnar spinel grains developed into an end member of alumina in a diffusion pair test at the places where Mg^{2+} and Al^{3+} were discovered to quickly counterdiffuse. This discovery demonstrated that columnar spinel grains formed at the original spinel-alumina interface before evolving into alumina. The center of curvature of the phase boundary between columnar spinel grains and the alumina end member, which was found in the latter, served as another justification for the interlayer's direction of propagation [12].

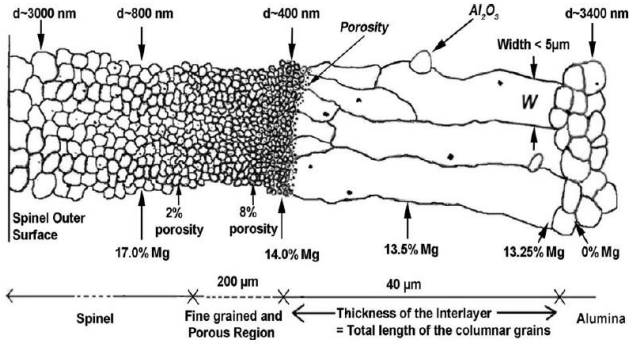

Figure 1.2. Schematic view of bi-material (alumina A-spinel) co-sintered during 16 hours at 1500 ºC [12].

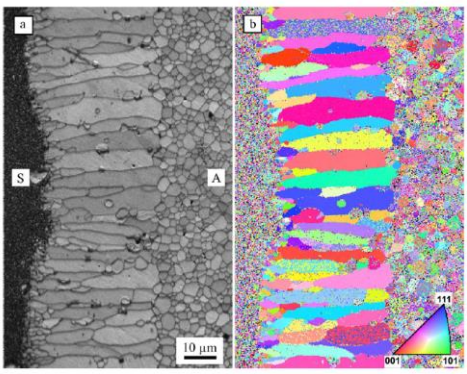

Figure 1.3. Microstructure and crystallographic view of spinel columnar grains formed during co-sintering at 1550 ^{o}C for 16 hours of alumina A–spinel bi-materials. (a) SEM image (b) inverse pole figure transverse direction = along the grain elongation with color coded map [12].

In the study mentioned above, microstructural development at the interface between alumina-spinel couple and their diffusive interactions were investigated. With the motivation stemming from this study, instead of forming alumina-spinel diffusion couples, in this thesis, it was attempted to coat the spinel structure on alumina pellets using the ESD method. The ability of the adhesion of the spinel coating on the alumina substrate and the coating conditions were investigated.

The main aims of this thesis are:

- To deposit spinel layer on dense alumina pellet by using electrostatic spray deposition method.
- To investigate the effect of parameters (nozzle to substrate distance, flow rate of precursors solution, applied voltage) on coating microstructure by conducting full factorial design experiments which enables to maximize the information with minimum number of trials.
- To select the optimum conditions in order to obtain a porous spinel microstructure on alumina substrate.

In Chapter 2 of this work, a detailed information about alumina and spinel structures, the other deposition methods, electrolytic spray depositon method, influence of ESD process parameters on coating microstructure and some studies on spinel deposited on alumina substrate and full factorial experimental design technique in the literature are discussed. The experimental procedure is explained in Chapter 3. The results

of the experiments and their discussions are given in Chapter 4. In Chapter 5, conclusions of the present work is stated.

CHAPTER 2

LITERATURE SEARCH

In this chapter, some insightful and detailed information about the ceramic materials, coating methods and electrospray deposition (ESD) in particular are given.

2.1. Ceramic Materials

Products manufactured from inorganic, nonmetallic materials that are first shaped and then hardened by heat are referred to as ceramics. The Greek term "keramikos," which means "pottery" or "burned substance," is the source of the English word "ceramics." There is also an older word coming from Sanskrit language which means “ material formed with the use of fire".This term covers a wide range of items, including nonmetallic magnetic materials, ferroelectrics, produced single crystals, glass-ceramics, refractories, structural clay products, abrasives, enamels, cements, and pottery, porcelain, and other materials [13].The main characteristics of ceramics are their brittleness, hardness, chemical, and thermal stability [14].

- **Structure and Properties of Ceramics**

The mechanical, thermal and other properties of ceramics are influenced by the present atoms, the way that the atoms packed and the bonding between these atoms. In ceramic materials, there are two types of bonding: Ionic and covalent. Ceramic materials contain both types of bonding, but the ionic bond predominates in the majority of them (especially the oxides). There are also materials possessing the mixture of both ionic and covalent bonding.

Ionic bonding, which is found in many ceramic materials such as NaCl, MgO and Al_2O_3, occurs between two elements with different capabilities of the nucleus of an atom to attract or retain the electrons. In other words, ionic boinding occurs between a metal and a non-metal which have different electronegativities. Instead, covalent bonds are formed when two nonmetals, or atoms with similar electronegativity, come together. In covalent bonds, the two atoms share electron pairs [15].

Ceramics have a crystalline structure, except for glasses which have an amorphous (non-crystalline) structure. The crystal structure and its properties can be affected by electrically charged ions and the magnitude of the electrical charges on each ionic component. The rationalization of the crystal structures of ionic compounds has been accomplished using Pauling's five rules (Table 2.1.) [16].

Table 2.1. Pauling's rules [16].

Radius Ratio Rule :	The coordination number of the cation is determined by the radius ratio of cation and anion.
Electrostatic Valence Rule :	In a stable coordination structure the electric charge of each anion tends to compensate the strength of the electrostatic valence bonds reaching to it from the cations at the centres of the polyhedra of which it forms a corner.
The Sharing of Edges and Faces :	The presence of shared edges, and particularly of shared faces, in a coordinated structure decreases its stability.
The Nature of Contiguous Polyhedra :	In a crystal containing different cations those with large valence and small coordination number tend not to share polyhedron elements with each other.
The Rule of Parsimony :	The number of essentially different kinds of constituents in a crystal tends to be small.

Figure 2.1 shows an example of the different crystal structures of some ionic materials and pozitively charged (cation) and negatively charged (anion) ions [17].

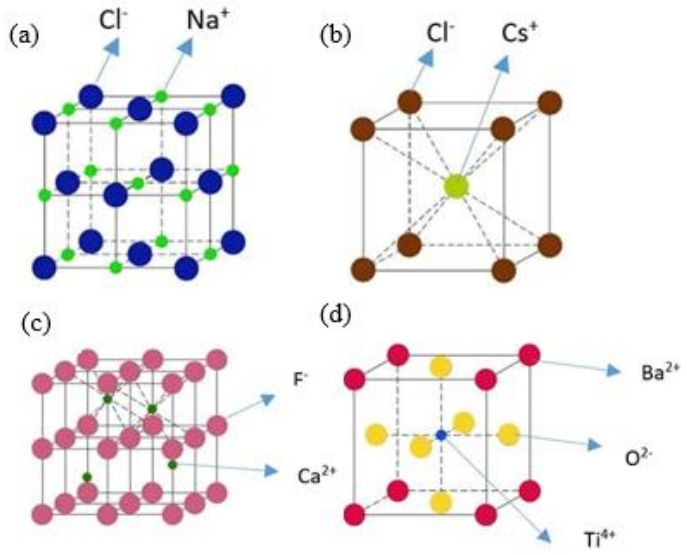

Figure 2.1. Various crystal structures of the ceramic materials: (a) NaCl (FCC), (b) CsCl (BCC), (c) CaF_2 (FCC), (d) $BaTiO_3$ (Perovskite) [17].

Therefore, ceramics have many promising properties due to their crystal structure. Typical properties of ceramic materials are listed: High dimensional stability, good wear resistance, high resistance to chemical attacks and corrosion, high melting point, high resistance to high temperatures, low thermal expansion, low to medium thermal conductivity, good electrical insulation, low to medium tensile strength, high compressive strength, poor impact strength, brittleness and low thermal shock resistance [15].

- **Categorization of Ceramic Materials**

There are many different classification schemes for ceramics with respect to their functions or their characteristics like the courseness or fineness. Figure 2.2 reveals the most general classification dividing them into two group as “Classical” and “Technical”.

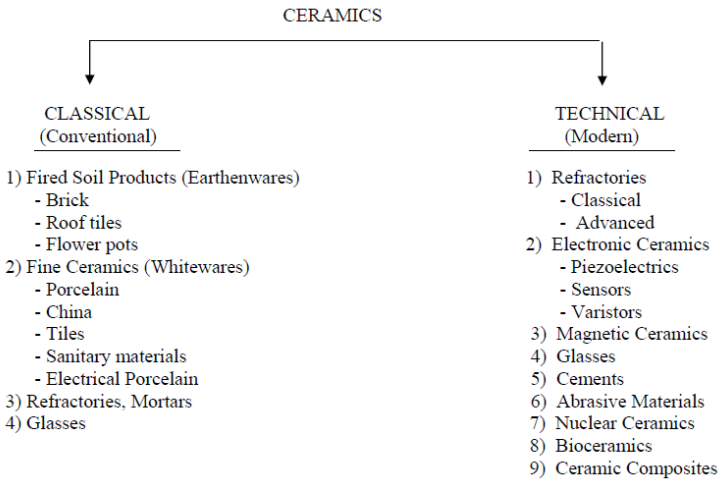

Figure 2.2. General classification for ceramics [13].

Classical ceramics which directly sources from the nature are manufactured from "triaxial" mixtures of clay + quartz + feldspar. For instance, quartz is a hard, crystalline mineral composed of silica (SiO_2). The chemical formula of $Al_2O_3.2SiO_2.nH2O$ refers aluminosilicate mineral which is also known as clay. Feldpar is with the chemical formula of $K_2O.Al_2O_3.6SiO_2$. Triaxial ceramics can therefore be thought of as combinations of the oxides K_2O, Al_2O_3, and SiO_2 for practical purposes. The reactions that will take place when these ceramics are fired require a thorough grasp of the phase equilibria in the K_2O-Al_2O_3-SiO_2 ternary system. Various porcelains, china, tiles, earthenware, sanitary ware, and similar other utilitarian ceramics are typical items coming under this category.

The majority of technical ceramics are non-triaxial and are made mostly from synthetic raw materials. This category includes ceramics used in mechanical, chemical, nuclear, thermal, biological, optical, electrical, electronic, magnetic, nuclear, and structural applications. Both oxides, such as Al_2O_3, MgO, CaO, TiO_2, ZrO_2, SiO_2, SnO_2, ZnO, PbO, NiO, Co, Cr_2O_3, B_2O_3, etc., and non-oxides can be used to make these products. The ceramics that are not oxides include nitrides such as Si_3N_4, AlN, and BN, borides such as TiB_2, ZrB_2, silicides such as $MoSi_2$, and halides such as NaCl, $MgCl_2$, CaF_2, and SrF_2. Chemically speaking, the end products could consist of a single oxide or non-oxide, mixed oxides like $PbZrO_3$-TiO_2 (PZT), or a solid solution of an oxide and a non-oxide like Al_2O_3- Si_3N_4 [13].

2.1.1. Alumina

Alumina or also known as aluminium oxide (Al_2O_3) is one of the most common ceramic materials for engineering applications. It can be also said that alumina is one of the widely used metal oxide due to its low manufacture cost. It has various areas of use in industry including the automotive, aircraft, medical and separation and purification technologies. It has been preferred and successfully used because of its strength, insulation characteristics, and, chemical and thermal stability. Alumina is an attractive ceramic material owing to its mechanical and thermal properties such as high hardness, wear resistance, resistance to high temperatures and corrosive environments, low thermal conductivity and chemical, high surface area, resistance to organic solvents, narrow particle size distributions, high density. Therefore, it is very advantageous for the production of automotive, aircraft and some high technology components as well as some electronic and medical devices. Nevertheless, although it has all these desirable properties, this ceramic material is quite brittle. Table 2.2 illustrates the alumina properties [18].

Table 2.2. Mechanical and thermal properties of alumina [19].

Tensile strength (MPa)	117-173	Melting point (^oC)	2051+/+9.7
Bending strength (MPa)	307-413	Thermal expansion coefficient at 200 ^oC-1000 ^oC ($^oC^{-1}$)	$8.80*10^{-6}$
Modulus of elasticity (E)$*10^8$ (MPa)	21.27-26.8	Boiling point (^oC)	3530+/-200
Compressive strength (MPa)	1600-3733	Hardness on the Mohs scale	9
Modulus of rigidity (G)$*10^8$ (MPa)	8.67-11.3		

Alumina possesses many different polymorps. These polymorps are high temperature phases which are δ-, κ-, θ-, α-Al_2O_3 and low temperature phases which are η-, γ-, χ-Al_2O_3. There is only one thermodynamically stable phase called α-Al_2O_3 (corundum). The other phases are metastable and they can be irreversibly turned into α-Al_2O_3 by thermal treatment of the related hydroxides such as gibbsite, bayerite, boehmite. These phases may differ in microstructure [4]. α-Al_2O_3 is the component in the formation

of a number of gems, including sapphire and ruby, the latter of which gets its blue hue from titanium and the former from chromium.

Figure 2.3 illustrates the crystal structure of alumina material. Alumina has a nearly hexagonal close-packed structure. The aluminium ions filling two-thirds of the octahedral interstices and the oxygen ions form this structure. It is seen that each aluminium ion center is in octahedral coordination [20]

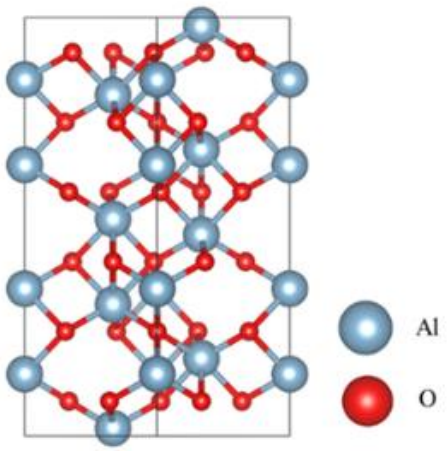

Figure 2.3. Hexagonal crystal structure of alumina (α-Al_2O_3) [20] .

α-Al_2O_3 is aluminum metal in its most oxidized state. That is why, more oxidation reactions are not possible for this phase. It can be said that it is quite stable in terms of physical and chemical. Al^{3+} and O^{2-} form strong chemical interactions that are both ionic and covalent, which give the material its high melting point, hardness, and resistance to the attack of powerful inorganic acids. Table 2.3 reveals some physical properties of alumina [21].

Table 2.3. Some other physical properties of alumina [21].

Property	**Value**
Crystallography	Hexagonal
Lattice parameter a	0.476 nm
Lattice parameter c	1.299 nm
Density (theoretical)	3.986 g/cm^3
Thermal conductivity (298 K, >99.9%TD)	30 W m^{-1} K
Specific heat (298 K)	8–10×10^{-4} J Kg^{-1} K

2.1.2. Spinel

The term “spinel” is used to refer a class of the double oxide whose general chemical formula AB_2O_4. The spinel group is mainly divided into three sub-categories in accordance with the industrial significance. These are aluminates, ferrites, and chromites. In this formula, *A* may be magnesium, iron, zinc, manganese, or nickel, and it may be combined with aluminum (aluminum-spinel), the magnetite (iron-spinel) in which B is iron, or the chromite (chromium-spinel) in which B is chromium [22].

One of the most important magnesia based-refractory materials is magnesium aluminate ($MgAl_2O_4$) spinel (MAS) [23] . It is a synthetic material which possesses cubic crystal structure. Figure 2.4 illustrates the crystalline structure of magnesium aluminate spinel. Al ions occupy octahedral positions, while Mg ions are seated in tetrahedral sites. The structure of MAS was modeled after that of a diamond. The A ions' locations resemble those of the carbon atoms in the diamond structure quite closely. This may account for the comparatively high hardness and high density that characterize this category. The other ions' configurations in the structure follow the symmetry of the diamond structure. None of the members of this group has cleavage directions.

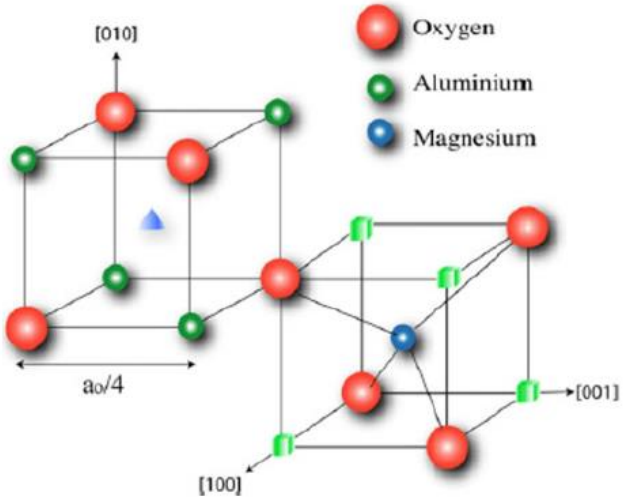

Figure 2.4. Crystalline structure of magnesium aluminate ($MgAl_2O_4$) spinel. Tetrahedral sites that are unoccupied are illustrated by (blue) triangles, while octahedral sites are displayed by (green) cubes [24].

Thanks to its magnificent chemical, thermal, dielectric, mechanical and optical properties, it has become an imperative material for optically transparent windows, domes and armours, and refractory applications. It has the best combination of many promising features such as high melting point, high hardness, relatively low density, high mechanical strength and, high resistance against chemical attack, wide energy band gap, high electrical resistivity, relatively low thermal expansion coefficient and high thermal shock resistance. Table 2.4 reveals the some important properties of magnesium aluminate ($MgAl_2O_4$)spinel [24].

Table 2.4. Some important properties of magnesium aluminate ($MgAl_2O_4$) spinel [24].

Property	**Value**
Melting point	2135^oC
Hardness	16 GPa
Density	3.58 g/cm^3
Mechanical strength (at room and at elevated temperatures)	135-216 MPa & 120-205 MPa at 1300 ^oC
Thermal expansion coefficient	9*10^{-6} $^oC^{-1}$ at 30-1400 ^oC
Thermal conductivity (at room temperatures)	24.7 W m^{-1} K^{-1}
Specific heat (at 20^oC)	0.21 cal g^{-1} K^{-1}

2.1.3. Magnesia-Alumina System

Magnesium aluminate ($MgAl_2O_4$) spinel is produced by the reaction of magnesium and aluminium oxides, because of the fact that deposits of $MgAl_2O_4$ does not exist naturally. These spinels which are commercially sintered can be magnesia rich, stoichiometric, and alumina rich. Magnesia and spinel structure have a large thermal expansion difference owing to high tensile hoop stress present around the spinel particles. That is why, magnesia- rich spinels generates too much cracking throughout the cooling process. Hence, the microcrack networks that formed around the spinel particles can be blamed for the increased resistance to thermal shock seen in the model magnesia-spinel composites [23]. Figure 2.5 displays the phase diagram for MgO and Al_2O_3.

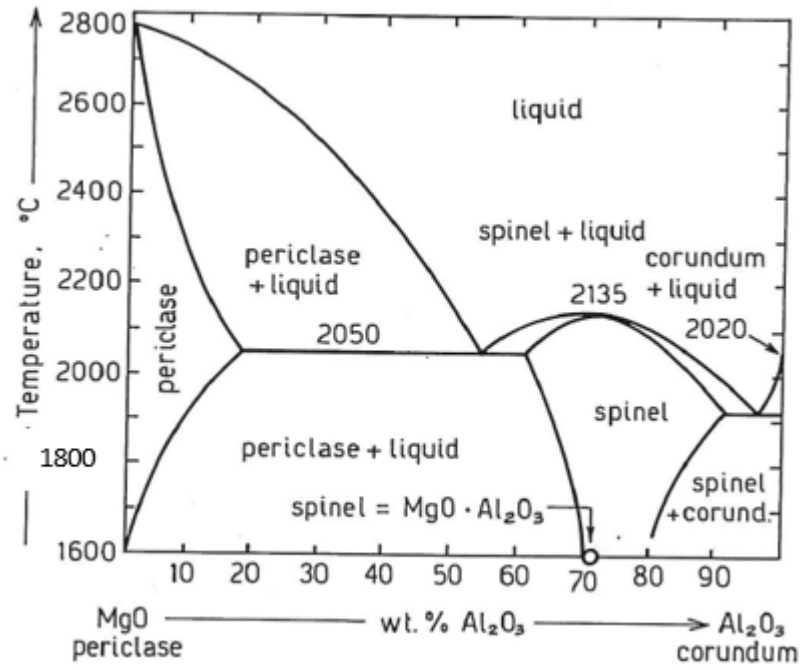

Figure 2.5. Phase diagram in the system MgO-Al_2O_3. Spinel melts congruently at 2135 ^oC and it is the only indermediate compound which melts at that temperature [25].

The stoichiometric MAS melts uniformly at 2135 ^oC and comprises 28.2% MgO and 71.8% Al_2O_3. Even though MgO has a relatively high melting point, a modest amount of MgO in Al_2O_3 significantly lowers its melting point. Additionally, two eutectic reactions as well as the intermediate phase $MgO.Al_2O_3$ exist. There aren't many terminal solubilities; for example, MgO is little dissolved by Al_2O_3 and vice versa. Therefore, for all intents and purposes, the pure end phases are the same as components. The MgO-Al_2O_3 system can also be thought of as two distinct phase diagrams, with MgO and $MgO.Al_2O_3$ for one and $MgO.Al_2O_3$ and Al_2O_3 for the other. The sole phase that develops at temperatures up to 1600^oC is $MgAl_2O_4$ spinel, which has a very wide range of stoichiometry. The solid solubility of MgO and Al_2O_3 in MAS is thought to be 2 and 6%, respectively, at this temperature. The solubility of these two oxides in spinel increases to 3.0 and 10.0%, respectively, when the firing temperature is raised to 1700^oC. The solid solution varies from 40 to more than 80% at 2000^oC. At roughly 1990 ^oC, the values of n in $MgO.nAl_2O_3$ span the range from less than 0.6 to larger than 7. However, it has been discovered that the pressure acting on MAS has a significant impact on its high temperature stability [24].

2.2. Ceramic Processing

In this sub-section, brief information about ceramic processing methods comprised by this thesis is provided.

2.2.1. Powder Properties

Ceramic processing generally starts from the powder obtained commercially. That is why, the knowledge of the powder's physical, chemical and surface properties is essential. The powder features such as size, size distribution, purity, shape, chemical compositon and level of agglomeration are some of the important ones.

- **Particle Size and Geometry**

Fine particles are convenient for an effective chemical reactivity. The typical particle size for powders used in processing of advanced ceramics is between 0.1-1 μm in diameter. These limits are determined by the thermodynamics of sintering for upper size limit and need to avoid particle flocculation for lower size limit.
Equiaxed or spherical particle geometry should be preferred to be able to control the uniformity of the packing.

- **Powder Defects and Impurities**

Powder defects like agglommerates causes non-homogeneous packing of the green body. Thus, this type of packing results in the different parts of the body to be sintered at different degrees.

Impurities is another concern to be kept at minimum level. Because they can create volume change, uncontrolled grain growth and undesirable phase transformations during the sintering and cracks during the cooling of the body.

- **Particle Size Distrubition**

High packing density is an important parameter limiting the shrinkage and distortion of the body during the firing. Broad particle size distrubition enhances the packing density and allows less sintering shrinkage and small pore size reduces sintering distance, and as a result, sintering temperture gets reduced, too.

2.2.2. Pressing

There are various methods to shape a ceramic body. The most common ways used in the traditional ceramic industry are listed in Table 2.5.

Water is the key element to select the proper method to form the ceramic body, because of the fact that the forming pressure required depend on the amount of the water in the body. In accordance with the relation between the water percentage and the shaping pressure, the suitable method can be determined [13].

Table 2.5. Common ceramic body shaping methods and water and pressure requirements for the related method [13].

Forming Method	**Water in the body (%)**	**Required forming pressure (atm)**
Dust pressing	0-2	200-1300
Dry pressing	5-10	60-1000
Isostatic pressing	0-15	300-700
Extrusion	15-20	30-700
Plastic forming	25-30	3-30
Slip casting	15-25	1

In this thesis, the uniaxial pressing method was used in order to form the ceramic body.

2.2.2.1. Uniaxial Pressing

Uniaxial pressing is the process of applying pressure in a single axial direction through a rigid punch or piston to mechanically compact a powder material contained in a rigid die. In the pressing cycle, a free-flowing ceramic powder is poured into a stiff die, compressed into a consolidated body, and then the consolidated body is ejected from the die as illustrated in Figure 2.6. The size and shape of the component to be pressed have a significant impact on the required pressure. Uniaxial presses can typically produce applied pressure that is comparable to 1 to 20 tons, while some presses are built to work at 100 tons. This method is undoubtedly easy, affordable, and appropriate for the mass production of ceramic parts. However, its uses are mostly restricted to compacting tiny and straightforward shapes like crucibles, tiles, bushings, and spacers. There are also some disadvantages of this method. These are vertical cracks, potential density variation and agglomerations. The main causes of these defecks and cracks are friction at the die wall and springback following ejection from the die. Cracks and defects might be eliminated, but not totally. By using a binder to increase the compact strength, applying lubricant to reduce die-wall friction, decreasing the applied pressure to minimize springback, and slowly releasing the pressure to slow down the rate of springback can minimize the effects [26].

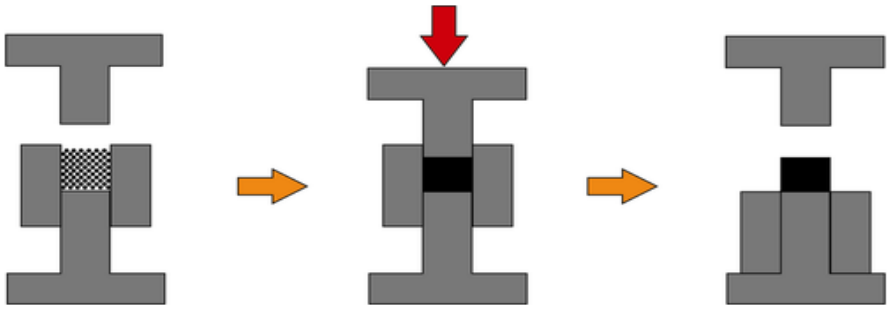

Figure 2.6. A schematic view of uniaxial pressing cycle [26].

The area with the most powder has a tendency to pack to a higher green density than the remainder of the body when powders are non-uniformly stacked in the die. Density

gradient may cause differential shrinking. Even when the die is evenly packed with powder, die wall friction can cause differences in compact density. During sintering, the agglomerates contract more than the surrounding body, resulting in porosity in the finished product. Contrary to common problems during pressing, non-uniform density difficulties are inevitable and typically do not become apparent until after the densification stage. Due to this, uniaxial pressing has only been applied to the fabrication of tiny, straightforward geometrical shapes or in situations where reliability is not essential [26].

2.2.3. Sintering

Ceramic materials are generally produced by starting from fine powders other than some exceptions like glass. The powder is milled, mixed or molded into the desired form by a lot of processes and then treated by heat or fired on the purpose of transforming them into a dense material. Sintering can be explained as a process using heat in order to assemble and bond powders to themselves in a chemical way and create a dense body. Sintering temperature is 1650 °C for alumina. However, sintering temperatures can change with respect to other parameters like particle size. After sintering, while the total surface of the powder and the bulk volume are decreased, the strength is increased.
If there is liquid phase forming during sintering, this is called liquid-phase sintering. Solid-state sintering is the term used for the case of the absence of a liquid phase.

The driving force throughout the sintering process is simply explained as the reduction of the excess energy related to the surfaces. There are two mechanisms resulting in the reduction of this excess energy and they are in competition. First one is the formation of the grain boundary area and destruction of solid/vapor interfaces leading to densification by grain growth. The second one is the coarsening due to the increase in the size of the particles. If densification dominates, the pores disappear by getting smaller and the compact shrinks. However, if the coarsening dominates, the pores and grains get larger. Figure 2.7 shows the two possible ways for the particles to reduce their excess energy [13].

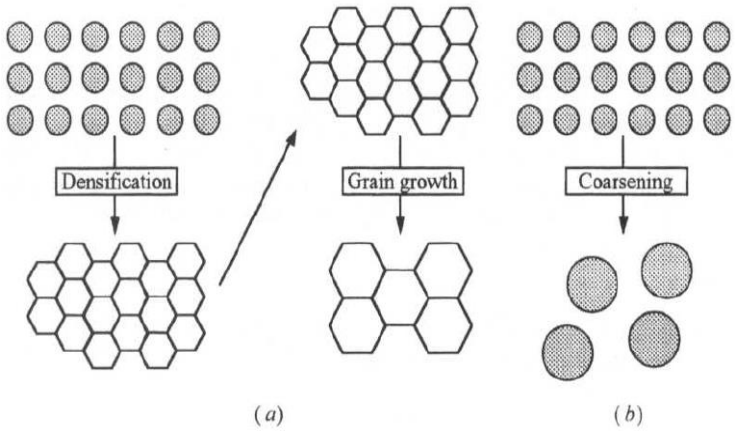

Figure 2.7. Illustration of (a) grain growth after densification and (b) coarsening [13].

"Interval of geometric change in which pore form is entirely determined (such as rounding of necks during the early stage sintering) or an interval of time during which the pore remains constant in shape while decreasing in size" is how an actual sintering stage is characterized. Three stages have been established based on this definition: an initial, an intermediate, and a final stage. Figure 2.8 shows these stages in solid state sintering [13].

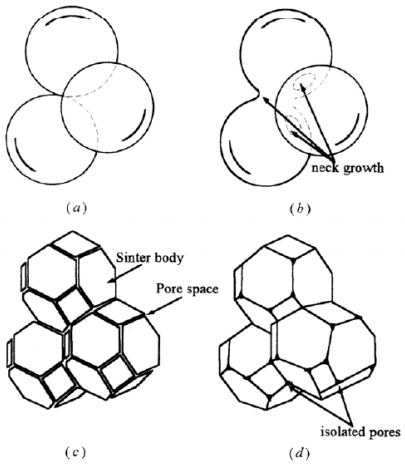

Figure 2.8. Stages in solid state sintering. (a) initial stage of sintering,

(b) almost end of the initial stage, neck growth is visible,

(c) intermediate stage, (d) final stage [13].

In the initial stage of solid state sintering, contact area of the particles grow and neck formation becomes visible. Grain boundary formation and neck growth at the

contact point and concave structure form. 10 % of densification is quickly (in seconds or minutes) completed in this stage due to strong driving force for sintering and large surface area.

In the intermediate stage, slow grain growth and neck growth cause a large reduction in mean porosity. Continuous pore channels that are aligned with three-grain edges define this level. Particles' centers come closer to each other and this results in compact shrinkage. The relative density rises from 70 to around 90–95%.

In the final stage, grain growth and porosity elimination start. All pores must be coupled to quick, direct diffusion pathways along grain boundaries in order for porosity to be completely eliminated during the final stages of sintering. An important feature of this stage is the rise in pore and grain boundary mobilities, which must be controlled if the theoretical density is to be reached [13].

Sintering process is driven by the reduction of surface free energy of aggregated particles. The reduction of surface free energy causes the material in the contact surfaces to distribute again. Sintering process provides a dense and almost pore-free microstructure. During sintering, many different mass transfer pathways can take place. Transport mechanism plays an important role on the atoms and the vacancy migration. Figure 2.9 illustrates the pathways that atoms and vacancies follow. These are surface diffusion, vapour transport through evaporation and condensation, grain boundary diffusion, volume diffusion (through the lattice) and plastic flow (vacancies coupling with dislocations) [27].

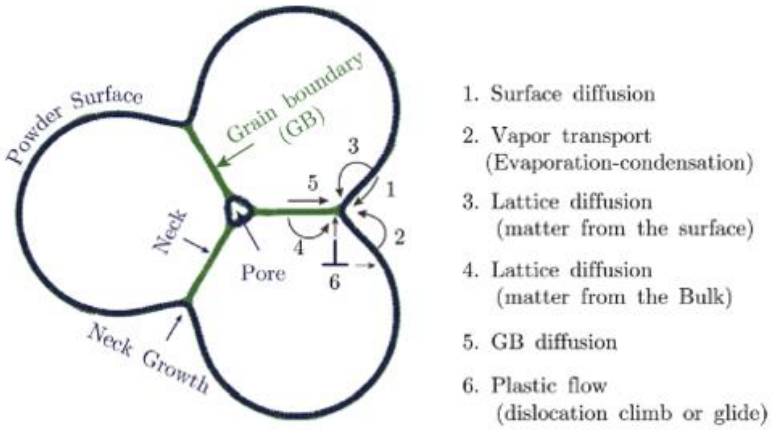

Figure 2.9. Various mass transfer pathways during solid state sintering [27].

2.3. Coating Methods

In this section, some deposition methods presented in the literature is explained.

There are plenty of techniques applied for creating and modifying deposited layers on different surfaces. Figure 2.10 illustrates the categorization of these techniques.

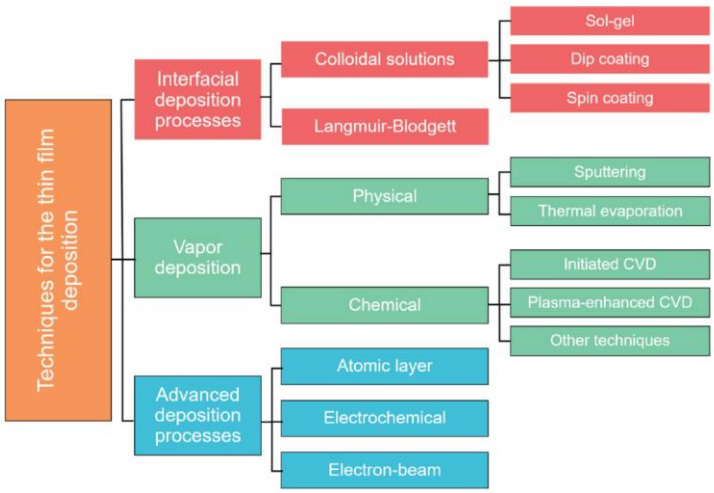

Figure 2.10. Categorization of deposition techniques [28].

2.3.1. Interfacial Deposition Techniques

These techniques benefit from the interfaces of different phases, for instance the water-air interface, to deposit layers on the surfaces. This technique is classified as Langmuir-Blodgett and colloidal solutions which is divided as sol-gel methods, spin-coating, and dip-coating [28].

Langmuir-Blodgett is a method of forming supramolecular body in ultrathin layers by controlling the crystal parameter and the formed structure [29]. This method uses the air-water interface to deposit monolayers [28]. It involves two fundamental steps. The first one is the development of the floating monolayer, so-called Langmuir film, at water-air interface and the second one is the coating of this film on the solid subsrate. The obtained structure is essential for applications of optical and molecular electronic devices [29].

Colloidal solutions including the reactants are deposited on the surfaces in the coating methods of sol-gel, dip and spin.

Sol-gel method has been widely used in coating processes of biomedical devices. Precursor solution called sol is prepared by dissolving calcium phosphorous in ethanol/distilled water. Gel phase is obtained from this solution by heating it at different temperatures. The substrate is dipped into this sol-gel phase at a fixed and controlled speed and can be repeated if multilayered or thicker coating is desired. Then, the deposited samples are baked or dried out faster in accordance with the intented microstructures of the coatings [30].

Sol-gel deposition techniques are constrained because a colloidal suspension of the precursors is necessary to create thin films (for example, through lengthy stirring in solution, frequently at a high temperature). Dip coating is a remarkably adaptable method for coating surfaces. It is highly flexible in terms of what can be coated but less so in terms of minimizing coating thickness. It is drenching the substrate in a precursor-containing solution before pulling it out quickly [28].

Spin coating is a popular technique that offers exceptional control over film thickness while depositing uniform films over flat substrates. With the exception of the centripetal force used in spin coating in place of the gravitational force used in dip coating, the process capabilities, coating qualities, and possible applications are essentially similar to those of dip coating. Greater control over the final film thickness is made possible by controlling rotating acceleration. Both techniques rely on a fluid dynamic equilibrium between a body force (gravity or centripetal) and forces from viscosity and surface tension [28].

2.3.2. Vapour Deposition Techniques

Vapour deposition techniques are classified as physical and chemical.

Physical vapour deposition (PVD) method creates a solid and dense layers on the target surface. The method is conducted in a high vacuumed media. Solid/liquid materials

are transferred by a vapour phase and after a metal vapour condensation, the desired coating is formed. Sputtering and evaporation are the most well-known types [30].

If the source material is converted into the vapour phase by evaporation, sputtering or through a carrier gas/plasma, the physical deposition method is named accordingly. The method can create electrically conductive and corrosion resistant deposits. It has a wide range of applications due to its flexibility and the availability of many different subsrates to be coated [28].

Chemical vapor deposition (CVD) methods transport a reactive vapor to a surface for deposition, just like PVD processes. In contrast to PVD, CVD involves deposition at the substrate and a chemical reaction that results in the chemical production of the desired coating. A substrate can achieve good adhesion to the relatively thin and homogeneous coatings created by CVD techniques.

By using a chemical initiator to kick off the polymerization process, initiated chemical vapor deposition differs from conventional CVD techniques.

Plasma-enhanced CVD (PECVD), also known as plasma deposition or plasma polymerization, is the most popular CVD method for changing the surface of polymers. Rather than temperature or a chemical initiator, the free radicals in the plasma act as the initiator in PECVD. When inert gas is exposed to a strong electric potential, which results in high electrical conductivity, a mixture of ordinary gas particles, radicals, ions, and electrons called plasma is created [28].

2.3.3. Advanced Deposition Techniques

Chemical gas-phase thin film deposition based on consecutive surface reactions is known as atomic layer deposition (ALD). It is distinguishable from other techniques by the unique pulsing approach, which grows the film layer by layer in a self-limiting manner. It is occasionally regarded as a type of CVD.

A process known as electrochemical deposition (ECD) involves depositing metals, oxides, or salts from an ion-containing solution onto an electrode, which conducts electricity. Three electrodes—a working electrode, a counter electrode, and a reference

electrode—are needed for the ECD process, which involves the reduction of metal ions at the working electrode as a result of current flowing through the solution.

Electron-beam techniques involve bombarding a target material with highly energetic electrons that pass through the target material. Free radicals are produced when electrons are displaced from their orbits, starting reactions. The energies that have been released have enough force to cut through the objects. Normal evaporative deposition procedures are improved in e-beam evaporation by the addition of an electron beam that warms the material target [28].

All these methods mentioned above have some advantages and disadvantages. They can be quite useful regarding to the their intend of use. However, they can also require relatively expensive equipments, careful and controlled labor work.

Next, electrostatic spray deposition method, which enables simplicity, cost effectiveness and flexibility of deposited surfaces, will be explained in detail.

2.3.4. Electrostatic Spray Deposition (ESD)

Electrostatic spray deposition (ESD) is a technique, which is also known as electrostatic spray pyrolysis (ESP) in the literature, is used in order to obtain dense or porous ceramic coatings [31], [32]. The configuration of an ESD set-up can be vertical or horizantal [31] . A vertical set-up mainly consists of a voltage generator, a syringe pump, a heating plate and a nozzle. Figure 2.11 illustrates the schematic view of the set-up [33].

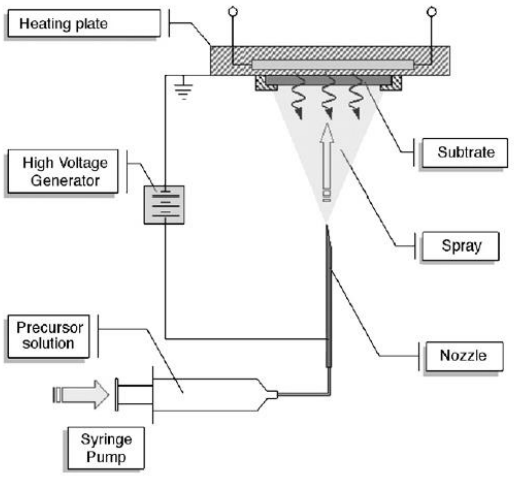

Figure 2.11. A schematic view of vertical ESD set-up [33].

This method possesses many advantages over the other deposition methods. These remarkable advantages can be listed as its simplicity, cost effectiveness, high deposition efficiency and the possibilty of use of a wide variety of non-toxic precursor solutions. As well as the features stated above, this technique enables to control the surface morphology of the coated layer easily and to tailor the ceramic deposition in a large variety [31], [33]. ESD is a spraying method which differs from the other spray deposition methods in terms of the spray of a precursor solution produced by an electrohydrodynamic (EHD) force [31]. The precursor solution is atomised by an electrical field to an aerosol. Then, the aerosol is moved through a heated substrate on which a deposited layer will form [32]. Therefore, the steps of ESD process can be listed in order as atomisation of the precursor solution at the nozzle tip, transport of the droplets between the nozzle and the substrate and formation of the deposit on the substrate surface. These are the steps affected by the process parameters. The main parameters are the substrate temperature, the distance between the nozzle and the substrate, the flow rate of the precursor solution and the atomisation voltage applied at the tip of the nozzle. Besides, there are also material parameters such as salts solubility, solvents' boiling point, solution surface tension, viscosity and conductivity [33].

The spraying modes of the aerosol generated by the electrical field depends on the applied voltage, the flow rate and the physical properties of the liquid. Different spraying

modes are represented in Figure 2.12 [34] .The most preferred mode is cone-jet among the other modes of electrostatic spraying due to the fact that it can generate single-sized droplets in the range of several micrometers. This mode involves the distortion of the liquid surface into a jet-extended Taylor cone. Another spraying mode is multi-jet mode. When the applied voltage is raised, this mode evolves from the cone jet mode. Cone jet mode is utilized for thin-film deposition more frequently than multi-jet mode. Cone-jet mode can be obtained in a relatively small range of applied voltages for each set of experimental conditions.

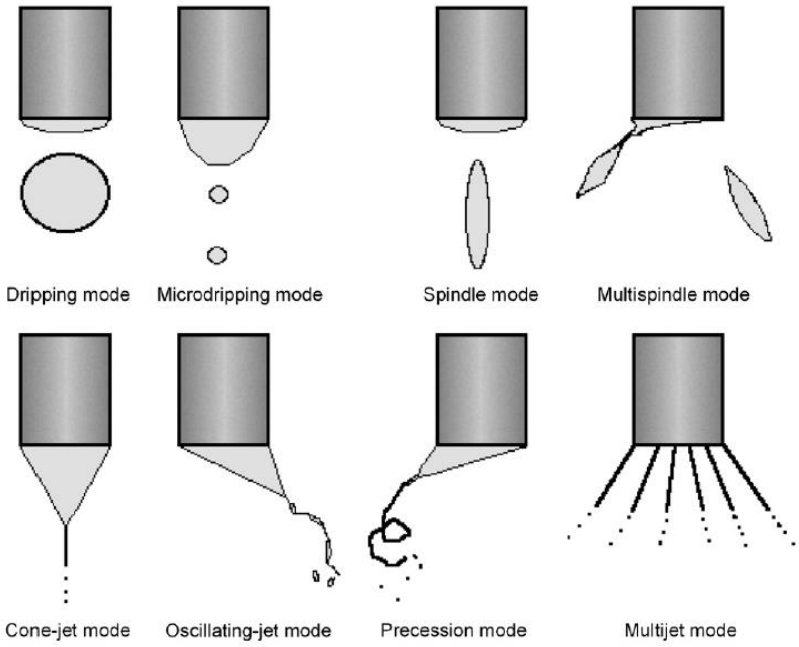

Figure 2.12. Different electro-spraying modes [34].

In ESD, morphology of the deposited layer is affected by numerous parameters. The way of spreading of the droplets on the substrate plays an important role. The porosity of the substrate is another influencer. The solvent with a high boiling point used in the precursor solution creates deposits with low porosity, while a solvent with a lower boiling point causes dense deposits.

Physical characteristics of the precursor solution affects the droplet size distrubution which can vary from about 10 to 100 μm and accordingly the structure of the deposit is also affected. The size of the droplets produced by electrostatic atomization can be calculated from the equation (1) below.

$$d \approx \sqrt[3]{\frac{\gamma \varepsilon_0^2}{\sigma^2 \rho}} \quad (1)$$

where γ is the surface tension, ε_0 is the electrical permittivity at vacuum, ρ is the density and σ is the conductivity of the solution [32].

Moreover, the chemical composition of the precursor solution has the control over the stoichiometry of the deposited layer. ESD enables to deposit a wide variety of microstructures on a substrate by tuning the parameters stated above [32], [35]. The size of the droplet and its interaction with the heated substrate ultimately determine the morphologic properties of the deposited layer [35].

Effects of ESD processing parameters on morphology of the coating is explained below.

- **Nozzle to Substrate Distance**

There is a temperature gradient produced between the substrate surface and the nozzle. During the flight of the droplets of the solution, evaporation occurred by reason of this temperature difference. As the nozzle to substrate distance increases, a large amount of the solvent will evaporate and coated particles will turn into smaller ones. These drier droplets landing on the substrate create a deposition layer which is better packad and dense. Droplet spreading is another important parameter in this regard. If the droplet is dry enough, when it contacts with the substrate surface, it will spread a little. However, if it possesses enough solvent, the impact will force it to spread on the surface before drying and solidifying in accordance with the configurations revealed in Figure 2.13. In this case, reticulated and cracked structure will be formed due to simultaneous boiling and drying of the droplets on the substrate surface when the temperature of the substrate is similar to the boiling temperature of the solvents. Cracks appear in consequence of the stresses produced by shrinkage of the deposit while the liquid evaporates on the surface [35].

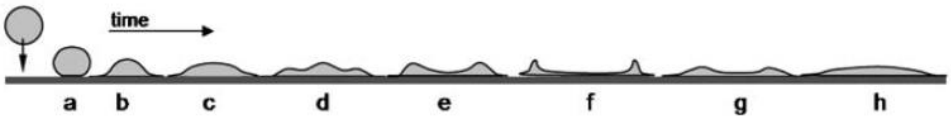

Figure 2.13. Stages of the droplet spreading on a continuous surface [35].

- **Flow Rate of the Precursor Solution**

Flow rate determine the initial droplet size. Whe the flow rate of the solution increases, the droplets forming at the tip of the nozzle will become larger. Larger droplets carry a large amount of solvent and they can go through long distances without getting dry completely. That is why, the microstructure of the film layer can vary accordingly both the combination of the flow rate and the flight distance which is the space between the nozzle tip and the substrate surface. It can be mentioned that relatively low flow rates will cause to cracked- free, dense and homogeneous porous layer owing to the smaller droplets generated at the tip of the nozzle [33], [35].

- **Deposition Temperature**

Deposition temperature is one of the parameters which affects the dynamic change of the droplet size during the flight. This change affects the spreading and drying of the droplets on the substrate relatively [35]**.** A continuous deposition layer can not form on the substrate when the rate of evaporation is greater than the rate of spreading [36]. The deposition temperature needs to be higher than the solvent evaporation temperature in order to induce porosity to occur on the films [35].

- **Deposition Time**

Kim et al. stated that the morphologies of the deposited layers changed toward a more porous structure as the deposition time increased. By taking into account the competitive impact, such as the rates of evaporation, decomposition, and spreading, they described this morphology. It was likely that the majority of the spray droplets that reached the substrate were still wet. Due to the substrate's often considerably higher surface tension than the solution, these droplets initially spread out across the surface of the substrate. Consequently, the solution droplets could spread quickly across the substrate's surface. A continuous deposition layer was established on the substrate because the rate of spreading was greater than the rate of evaporation [36].

- **Nature of the Precursor Solution**

Neagu et al. obtained zirconia-based coatings by using ESD technique. For the purpose of investigating the effect of the nature of the precursor solution, they used two different solutions on the substrates. The former was zirconyl nitrate (ZrO(NO3)2) based solution and the latter was zirconium acetylacetonate Zr (C5H7O2)4. The authors stated that zirconyl nitrate could be a favorable precursor due to its high solubility and fast thermal decomposition. Besides, high conductivity of the solutions is a drawback, because it causes tiny droplets to form and consequently to highly porous deposits. This can be avoided by using a solvent mixture with a high boiling point. Oppositely, zirconium acetylacetonate decomposed more slowly and yielded a low conductivity. Therefore, it was suitable to be coated at relatively high temperatures in order to obtain dense and smooth depositions [32].

- **Solvent Mixtures**

Because salts are more soluble in mixes of solvents than in pure solvents and because they evaporate over a wider temperature range, there is a decreased danger of drying cracks in mixtures of solvents. The boiling interval of solvent mixtures is crucial

information. The amount of liquid that contacts the substrate and its rate of evaporation depend on the boiling interval [32]. If the solution is decomposed faster, charged droplets are atomised faster. Before landing on the substrate surface, evaporation of the solvent during the flight takes place. Therefore, agglomerations on the substrate surface can be observed [37].

- **Concentration of the Precursor Solution**

The conductivity of the precursor solution increases with its concentration. Therefore, smaller droplets will fully dry during the travel toward the substrate and the preferential landing's influence will be stronger. Low-conductivity precursor solutions can be used to offset the effects of concentration [32].

- **Nature of the Substrate**

As long as the open pores were in the micrometer range, the morphology of the coatings is not significantly affected by the nature of the substrate surface. If there are deep and larger pores, they cannot be covered continuously [32]. However, another study stated that density, surface roughness and tension of a substrate can affect the microstructure of the deposition. Because of different feature of the coated layer, these properties can vary. Porous structure of the substrate might influence the coating due to lower thermal conductivity. Low thermal conductivity also reduces the heat required for solvent evaporation close to or at the substrate surface. A high surface roughness will promote the droplets' preferred landing and produce more agglomerates. Discrete particles may arise as a result of low surface tension. Additionally, this makes the surface rougher, which makes it more likely that the droplets will land preferentially [38]. Preferential landing effect is defined in the literature as the solidification of the particles and overlapping during the deposition due to the prematurely evaporation of the solvent’s droplets during the relatively long flight from the nozzle tip to the substrate surface [37]

- **Applied Voltage**

One of the studies in the literature claimed that spraying mode varied in accordance with the applied voltage. In order to obtain workable spraying modes such as dripping or cone jet mode, the voltage had to be increased, because voltages less than 7 kV failed to create aerosol particles. As soon as the voltage varied, the spraying modes also varied from dripping mode to cone jet mode. A further increse of the applied voltage resulted in a change from cone jet to multi-jet mode leading to aggregated layers on the substrate surface. The formation of cone jet mode of spraying created homogenous and well-dispersed depositions. Dripping mode of spraying caused to cracked and non-homogeneous surface because of the fact that the droplets formed reached the substrate surface and most of the evaporation occurred there, not during the flight from the tip of the nozzle to the target surface. The droplets obviously flew towards the surface without control and engendered cracks and non-homogeneity [37].

2.3.5. Comparison of Coating Methods

A good coating deposition on a substrate depends on a number of factors, including the feedstock form (powder, wire, rods, precursors, etc.), the substrate material, the deposition technique, and the deposition materials. Numerous different type of coating techniques have been introduced in the literature so far. Even if each of these methods has benefits, their use is always constrained by limitations. In Table 2.6, some of the common coating methods' advantages and disavantages are listed [30].

Table 2.6. Advantages and disadvantages of some main coating processes and their comparison with ESD technique [30], [37], [39].

Coating method	**Advantages**	**Disadvantages**
Vapour deposition techniques	• Corrosion and wear resistance • Possiblity of thin film deposition • Deposition of various types of materials with different microstructures • Possibility of working with low pressures	• Requires high vacuum • Corrosion resistance is affected by abrasion • Degration control can be challenging • Requires heat resistance substrates.
Thermal spraying	• Corrosion and wear resistant coatings • Thick coating	• Requires a heat source • Limited operation range.
Sol-gel	• Cost effective biomedical applications • Providing corrosion and ion release protection • Multilayered (thick) coating • High adhesion • Ability to coat complex geometries • Flexibility in the composition • No need of conductive substrates	• Thickness control • Slow rate of coating cycle • Possibility of coating failure during heat treatment on multilayered coating structures
Electrostatic spray deposition	• Possibility of control of surface morphology • Wide variety of coating microstructures (dense and porous) • Simple and easy to operate • Cost effective • High deposition rate • Availability of non-toxic feedstock form	• Poor adhesion to the surface. • Amorphous coatings, required post heat treatment.

Apart from the advantages and disadvantages of these coating methods, each method allows to obtain coatings with different microstructures. Figure 2.14 reveals the different coating morphologies obtained by different coating techniques.

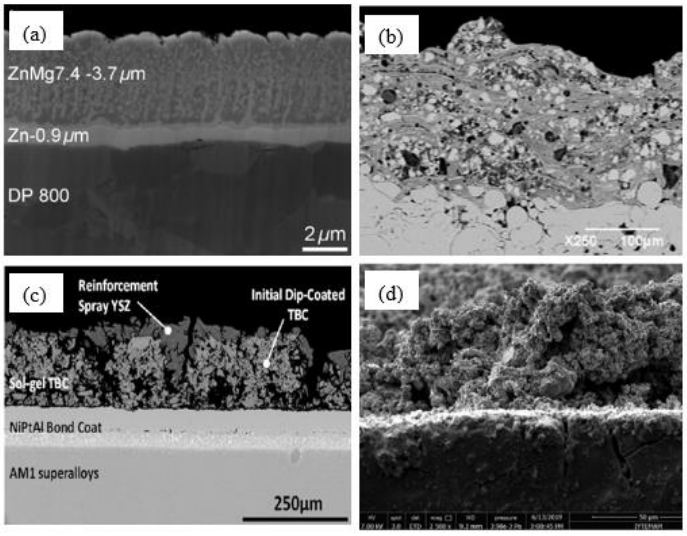

Figure 2.14. Different deposition morphologies obtained by common coating techniques. (a) ZnMg-Zn bi-layered coating by physical vapour deposition [40], (b) Zirconia-alumina/ alloy based on Ni by thermal spraying method [41], (c) Sol–gel thermal barrier coating [42], (d) LSCF layers deposited on GDC electrolyte by ESD [37].

Physical vapour deposition technique provides multilayered coatings with variable compositions for protection purposes such as being protective to atmospheric corrosion and accurate thickness control of these coatings. Besides, they are also used to improve adhesion performance of the surface. PVD coatings have columnar microstructure with elongated grains and grain boundaries as it is seen in Figure 2.14. By adjusting of the microstructure of these elongated grains, insulation properties of the deposited layer can be improved [40], [42].

Thermal spraying method produces metallic coatings, ceramics, polymers and composites in order to protect structures from high temperatures. They work as a thermal barrier. The resulting coatings can be defined as thin coatings with a low thermal conductivity and they have a high resistance to thermal shock. Typical characteristics of these deposited layers are being lamellar with non-molten or semi-molten particles and cracks as shown in Figure 2.14 [41].

Sol-gel thermal barrier coatings are inherently microcracked because production process contains heat treatment. They show a specific isotropic microstructure with randomly distributed porosities as presented in Figure 2.14 [42].

ESD technique used for coating cathode layers on electrolytes of intermediate temperature solid oxide fuel cells (IT-SOFC) can create coral like structure with nano-porosity as reveal in Figure 2.14 [37].

2.4. Studies on $MgAl_2O_4$ Spinel Coated Alumina Substrates in the Literature

There are plenty of different techniques proposed in the literature to create coatings of various materials on many different kind of substrates. In this part of the study, a few examples of studies which demostrated formation of $MgAl_2O_4$ spinel coatings on alumina substrates by discrete deposition methods are discussed.

$MgAl_2O_4$ spinel draws interest in many different industrial applications due to its desirable properties such as high resistance to attack, low electrical loss. It provides promising features physically, chemically and thermally. Therefore, it is convenient to be used as a refractory lining in steel-making furnaces, transition and burning zones of cement rotary kilns [43]. $MgAl_2O_4$ spinel is also an attractive composite metal oxide. Therefore, there has been a growing interest of synthesis of 1D $MgAl_2O_4$ spinel nanostructures. It is expected to be useful for production of electrical and catalytic nano devices and to be used as an additive in order to provide new and improved functions to nanocomposites.

For this purpose, Jeong et al. studied the direct synthesis of 20 nm of $MgAl_2O_4$ spinel nanowires on an Al coated- alumina substrate at 800 ^oC through a continuous vapor–solid growth mechanism.

First of all, Al coating was performed on Al_2O_3 substrate by a multi-metal sputtering machine. Then, a suspension containing MgO nanoparticles and ethanol was ultrasonicated and it was coated on the surface of the Al-coated Al_2O_3 substrate using a spray apparatus with a nozzle. The prepared subsrates were further placed at the center of

a quartz reactor heated to 800 ^{o}C with a rate of 30 ^{o}C/min in Ar. It was assumed by the authors that $MgAl_2O_4$ spinel nanowires on an Al coated- alumina substrate would have an important impact on the fields of ceramic and chemical reaction engineering [44].

Aluminum metal matrix composites reinforced by ceramic particles is favorable material to be benefited from in the car and aerospace industries thanks to their high specific strength and temperature creep resistance and wear resistance. $MgAl_2O_4$ spinel has also been used as reinforcement due to its important features.

Chen et al. in-situ coated a polycrystalline layer of nano-$MgAl_2O_4$ spinel on the surface of nano-sized alumina particles (Al_2O_3np) by electroless plating and calcination process in their study. Then, hybrid of $MgAl_2O_4$-coated Al_2O_3np and $MgAl_2O_4$ particles were used as a reinforcement for aluminum matrix composites. They prepare these composites by the help of high intensity ultrasonic assisted casting method. Ultrasonic vibration and particle wetting have an influence on nanoparticle entering the melt and dispersion mechanism. Based on this knowledge, they aimed to control the size and distribution of nanoparticle in the matrix for the purpose of formation of composites with higher performance. Besides, they proposed a model of particle migration under ultrasound treatment [45].

The use of structured materials as catalyst support has gained importance recently because of their benefits on the reactions required high temperatures such as catalytic dehydrogenations and partial hydrogenations processes which can be encountered in petrochemical industry. $MgAl_2O_4$ spinel is an interesting alternative for catalysts supports due to its low acidity and ability to spread and stabilize the supported metals well. It was stated that there was pratically no information about $MgAl_2O_4$ spinel coating on alumina spheres in the literature. For this purpose, Baez et al. proposed a novel coating method of $MgAl_2O_4$ spinel on alumina spheric nuclei.

Porous and thin layers of spinel was coated on α-Al_2O_3 spheres by a method including a precursor gel of $MgAl_2O_4$ by citrate-nitrate combustion. α-Al_2O_3 spheres pretreated with HCl was mixed with solution of citric acid, aluminum nitrate and magnesium nitrate and heated until boiling. Then, gel formation was observed and gel+spheres were dried in vacuum. Subsequently, the obtained structure was calcinated with N_2 and N_2/O_2 [46].

Voigt et al. prepared functionalized alumina filters coated $MgAl_2O_4$ spinel by using two different coating methods: Spraying and dipping of the filter into the slurry.They investigated the homoegeneity of the coating and the cold compression strength of the coating. They studied different number of sintering steps and coating methods as spraying and dipping combined with centrifugation while preparing the samples [47].

Plenty of methods were investigated to coat spinel on alumina substrate for several purposes as stated in the literature. In this thesis, for the first time, spinel deposited on alumina material by ESD technique was studied.

2.5. Full Factorial Experimental Design

In this thesis, full factorial design experiments were conducted for the purpose of maximizing the information with minimum number of trials.

Factorial design is a research strategy that allows researchers to look into the main and interaction effects of two or more independent factors on one or more outcome variables [48].

It can be said that in many experimental studies, there are two or more independent factors affecting the result of that study. By applying a factorial design strategy in these kind of researches, one can obtain efficient results and comment on them sufficiently. In a factorial design, all possible combinations of the levels of those factors or independent variables are worked on in each trial or replicate of the experiment if it is desired to be conducted. For instance, the effects of the weather temperature and the exposure time to the sunlight on growth of a flower would like to been investigated. There are two levels for the weather temperature as 20 C and 40 C. The levels for the exposure time to the sunlight are 2 hours and 8 hours in a day. For this example, each replicate of the experiment includes 2*2 equaling 4 combinations. The effect of the factors is the change of the response/ output. This is also called dependent variable. The factors can be defined as independent variables.

Several particular examples of the general factorial design, on the other hand, are significant because they are frequently employed in research and also serve as the foundation for other designs with significant practical significance.

The most important of these specific examples are k factors, which have only two levels apiece.

These levels can be quantitative, such as two temperature, pressure, or time values, or qualitative, such as two machines, two operators, a factor's "high" and "low" levels, or even the existence and absence of a factor. Simply, such a design has always a fixed value of two levels, but the number of factors are changeable accordingly. Therefore, this requires 2*2*2*….*2k observations or trials for each replicate of the experiement and is called 2k factorial design. Because, there are only two levels per factor, the response can be assumed to be linear over the the range of the factor levels.
This kind of design is very useful in the early stages of an experimental study. This method provides the smallest number of trials. That is why, these designs are widely used [49].

2.5.1. Analysis of Variance (ANOVA)

In this thesis, ANOVA analysis were done in order to investigate the effect and significance of the independent variables (working distance, applied voltage and flow rate of the precursor solution) on obtaining a porous layer on the alumina subsrates.

Analysis of variance, in short ANOVA, is defined as a statistical method which divides observed variance data into various components for use in further testing. It is used for obtaining information about the relationship between the dependent and independent variables.

ANOVA can be simply categorized into two sub-sections: One way ANOVA and factorial ANOVA.

One way ANOVA is used when there is only one independent variable. Factorial ANOVA differs in the number of dependent variables. There must be at least 2 independent variables with at least two levels for factorial ANOVA. This type indicates whether both the main effect and the joint effect (interaction) are significant [50].

The p value obtained as a result of ANOVA shows the degree of influence of the analyzed independent variables or the significance level on the dependent variable statistically. It can be simply explained that if a p value is 0.10 or less, the influence of that independent variance, or the effect of two or more independence variances together are significant. This means they have a quite impact on the dependent variable [51].

CHAPTER 3

EXPERIMENTAL

In this section, the experimental procedures followed during the thesis and the materials used in the experiments are presented. In the first part, materials and equipments used in the experiments are explained. In the second part, the experimental set-up and procedures are discussed in reference to literature. In the third part, characterization analysis plan and the preparations for these analysis are presented.

3.1. Materials and Equipments

There were mainly two different types of materials used in the thesis: Ceramic pellets and the coating. The former was made from high purity alumina as explained below. The latter was made using polymeric precursor solution bearing the necessary cations of $Mg^{2+,}$ Al^{3+} or Cr^{3+}.

ESD set-up was used to create the coatings on the ceramic pellets.

3.1.1. Alumina Powder

Alumina powder (Alcoa CT3000SG) was obtained from Alcoa, Inc and had the properties listed in Tables 3.1 and Table 3.2.

Table 3.1. Alcoa CT3000SG alumina powder properties [52].

Properties	**Typical**
Specific surface area / BET	7.80 m^2/g
Particle size /D50 Cilas	0.5 μm
Particle size /D90 Cilas	2.0 μm
Green density (90 MPa)	2.94 g/cm^3
Fired density (1540 ºC /1600 ºC)	3.91 g/cm^3 / 3.95 g/cm^3
Shrinkage (1540 ºC /1600 ºC)	16.8% / 17.3%

Table 3.2. Alcoa CT3000SG alumina powder chemical analysis [52].

Chemical Analysis	**Typical (%)**
Al_2O_3	99.8
Na_2O	0.03
Fe_2O_3	0.015
SiO_2	0.015
MgO	0.040
CaO	0.015

3.1.2 Polymeric Precursor Salts

Polymeric precursor solutions were prepared using salts of Al, Mg or Cr. For Al^{3+}, analytical grade $Al(NO_3)_3.9H_2O$ (Sigma Aldrich, Germany, >98% purity, CAS: 7784-27-2) and analytical grade $Mg(NO_3)_2.6H_2O$ (Panreac, Italy, >98% purity, CAS: 13446-18-9) was used for Mg^{2+}. In order to obtain Cr^{3+}, analytical grade $Cr(NO_3)_3.9H_2O$ (Alfa Aesar, Germany,98.5 % purity, CAS: 7789-02-8) was used.

3.1.3. ESD Set-up

Precursor solutions were sprayed onto the sintered alumina pellets using a vertical ESD set-up which mainly consists of a syringe pump, voltage supply and a heater. Figure 3.1 reveals the basic schematic view of the ESD set-up.

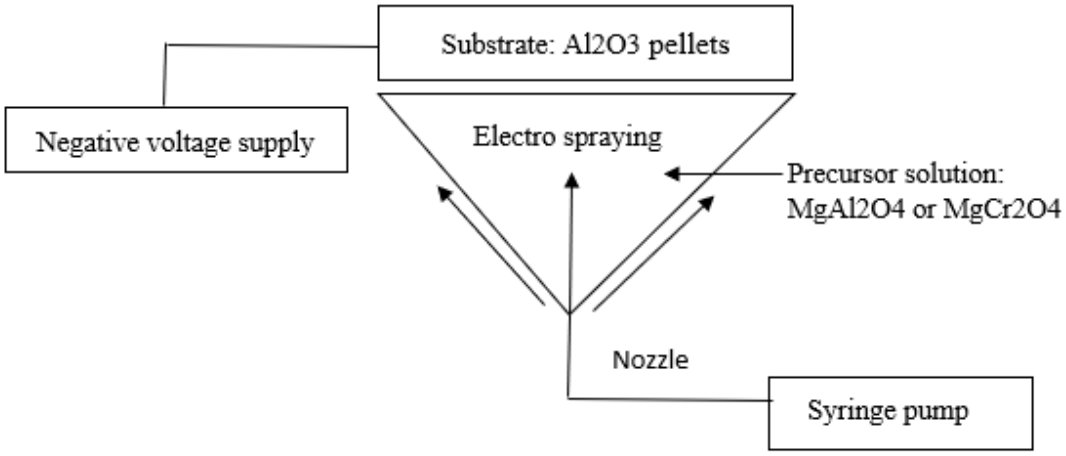

Figure 3.1. Simple schematic view of ESD set-up.

3.2. Experimental Procedures and Plan

In this section, the preparation of the alumina pellets and polymeric precursor solutions are explained. Coating procedure is also presented. To investigate the microstructures of the coatings and the precursor solutions, SEM, EDX and XRD analysis were performed. The preparation procedures of the coatings and the solutions for the analysis stated above are discussed.

3.2.1. Preparation of the Substrate: Aluminum Oxide Pellets

1 g of the powder was weighed and poured into the mold. It was mixed with 1-2 drops of ethanol in the mold and compacted manually by uniaxial pressing in a stainless-steel die with 13 mm of diameter and then pressed by a hydraulic press (Carver, Wabash, IN, USA) at 100 MPa, then de-aired, pressed one more time at 250 MPa. The pellets were then placed in a box kiln (Nabertherm LHT 02/17, Germany) and heated to 110 °C and soaked for 1 hour for drying followed by heating at a rate of 3^{o}C/min up to 1500 °C with a soak time of 1 hour. After soaking at the target temperature, the furnace was cooled to room temperature at a rate of 3^{o}C/min. Sintered samples were around 12.7 mm in diameter and 2 mm of thickness. The pellet was found to linearly shrink by 3 %.

- **Preparation of Bisque-fired Aluminum Oxide Pellet**

For the purpose of preparing a bisque-fired alumina pellet, the same steps mentioned in the section **3.2.1** was followed. The only difference was the sintering procedure. The bisque-fired pellet was heated up to 1100^{o} C with a rate of 10 ^{o}C/min with a soak time of 1 hour. After soaking at the target temperature, the furnace was cooled to room temperature at a rate of 10^{o}C/min. The bisque-fired pellet was around 13 mm of diameter and 2 mm of thickness. The pellet was observed not to shrink at all. Figure 3.2 shows the alumina pellets after sintering.

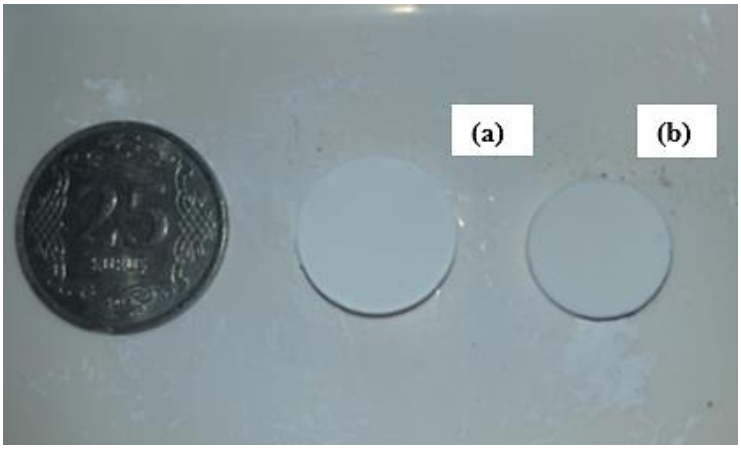

Figure 3.2. Alumina pellets after sintering. (a) Alumina pellet sintered at 1100^{o} C and (b) alumina pellet sintered at 1500^{o} C.

3.2.2. Preparation of Precursor Solutions: $MgAl_2O_4$ and $MgCr_2O_4$ Spinel Groups

In order to form a spinel structure, precursor solutions which included Mg^{2+}, Al^{3+} and Cr^{3+} ions were prepared. Salts of analytical grade $Mg(NO_3)_2.6H_2O$ and $Al(NO_3)_3.9H_2O$ and $Cr(NO_3)_3.9H_2O$ were dissolved in ethanol C_2H_5OH (Merck KGaA, Germany, CAS: 64-17-5) and diethyleneglycolmono- butylether, also known as butylcarbitol($CH_3(CH_2)_3OCH_2$- $CH_2OCH_2CH_2OH$ (Alfa Aesar, Germany,99 % purity, CAS: 112-34-5) with a 1:2 volume ratio. Table 3.3 shows the proportion of salts and solvent for all solutions.

Table 3.3. Proportions of the salts and solvents for all solutions. The volumes of ethanol and butyl carbitol used in all solutions were 33.33 and 66.67ml, respectively.

Solution	**$Mg(NO_3)_2$. $6H_2O$**	**$Al(NO_3)_3$. $9H_2O$**	**$Cr(NO_3)_3$. $9H_2O$**	**Molarity**
Mg-rich- $MgAl_2O_4$	0,005 mol	0,005 mol	-	0,025 M
$MgAl_2O_4$	0,0025 mol	0,005 mol	-	0,025 M
$MgCr_2O_4$	0,0025 mol	-	0,005 mol	0,025 M

3.2.3. Coating Procedure by ESD

Sintered alumina pellet (substrate) was placed between two aluminum plates, on a 10 mm diameter hole located in the center of the bottom aluminum plate. Glass wool was covered around the plates in order to keep the plate temperatures constant throughout the experiment and to prevent temperature loss while heating the plates. The substrate temperature was expected to be maintained at 300°C by an electrical resistance heater (ENDA, Digital PID Thermostat). The polymeric precursor had to be heated to guarantee that the solvents inside had completely evaporated and that any leftover cations had formed coatings on the pore surfaces [37]. The temperature rise was continuously observed with the help of a thermocouple placed between the plates. After the temperature of the plates reached 300°C, the 0.025 M of precursor solution (Mg-rich- $MgAl_2O_4$) was filled into the syringe (Ayset, 10 mL, syringe with a metallic hypodermic needle). Since

hypodermic needle tips typically have an angle-cut shape, they were chopped using a Dremel Tool to create a blunt tip to improve spraying conditions. The needle had an outside diameter of 0.50 mm [37]**.** The syringe filled with the precursor solution was placed on the syringe pump (NE-300, USA, Serial no: 283686) which provided the controlled flow rate. The desired distance was set by measuring the distance between the needle tip of the syringe and the pellet. In order to observe Taylor cone formation throughout the experiment, the camera was positioned to see the area to be sprayed. In order to provide electrical current to the system, the negative end of the voltage power supplier (PULSElectronic, Turkey) was placed on one of the plates and the positive end on the needle tip of the syringe. Next, the voltage power supplier was started and the desired voltage was set. Spraying was done for 10 minutes for each experiment.

By using full factorial experimental design, the distance between the pellet and the needle tip, applied voltage and flowrate of the precursor solution, which are the parameters affecting the coating morphology, was changed and 8 different experiments were carried out as stated in Table 3.4.

Table 3.4. Full factorial experimental design for coating of spinel layer by ESD technique and the design parameters. Spraying time was 10 minutes and temperature of the substrate surface was 300^{o} C. 0,025 M of $MgAl_2O_4$ spinel precursor solution was sprayed for each.

Experiment Number	**Working distance (mm)**	**Flow rate (ml/h)**	**Voltage (kV)**
1	15	0,25	6
2	15	0,25	10
3	15	0,1	6
4	15	0,1	10
5	25	0,25	6
6	25	0,25	10
7	25	0,1	6
8	25	0,1	10

While the distance between the pellet and the needle tip, the flow rate of the precursor solution and applied voltage were varied in accordance with full factorial experimental design plan, the other parameters affecting the coating quality such as spraying time, heating plate temperature/temperature of the substrate surface and the concentration of the precursor solution were kept constant.

Other than the experiments stated in Table 3.4, $MgAl_2O_4$ spinel solution was coated on both the alumina pellet sintered at 1500 ^oC and the bisque-fired pellet (sintered at 1100 ^oC) by following the coating procedure described in section **3.2.3** using the number 1 experimental conditions.

Besides, $MgCr_2O_4$ spinel coating was also carried out on the alumina pellet sintered at 1500 ^oC with the same procedure as in section **3.2.3** using the number 1 experimental conditions.

3.2.4. Experimental Plan

Experimental plan followed in this thesis is illustrated in Figure 3.3 below.

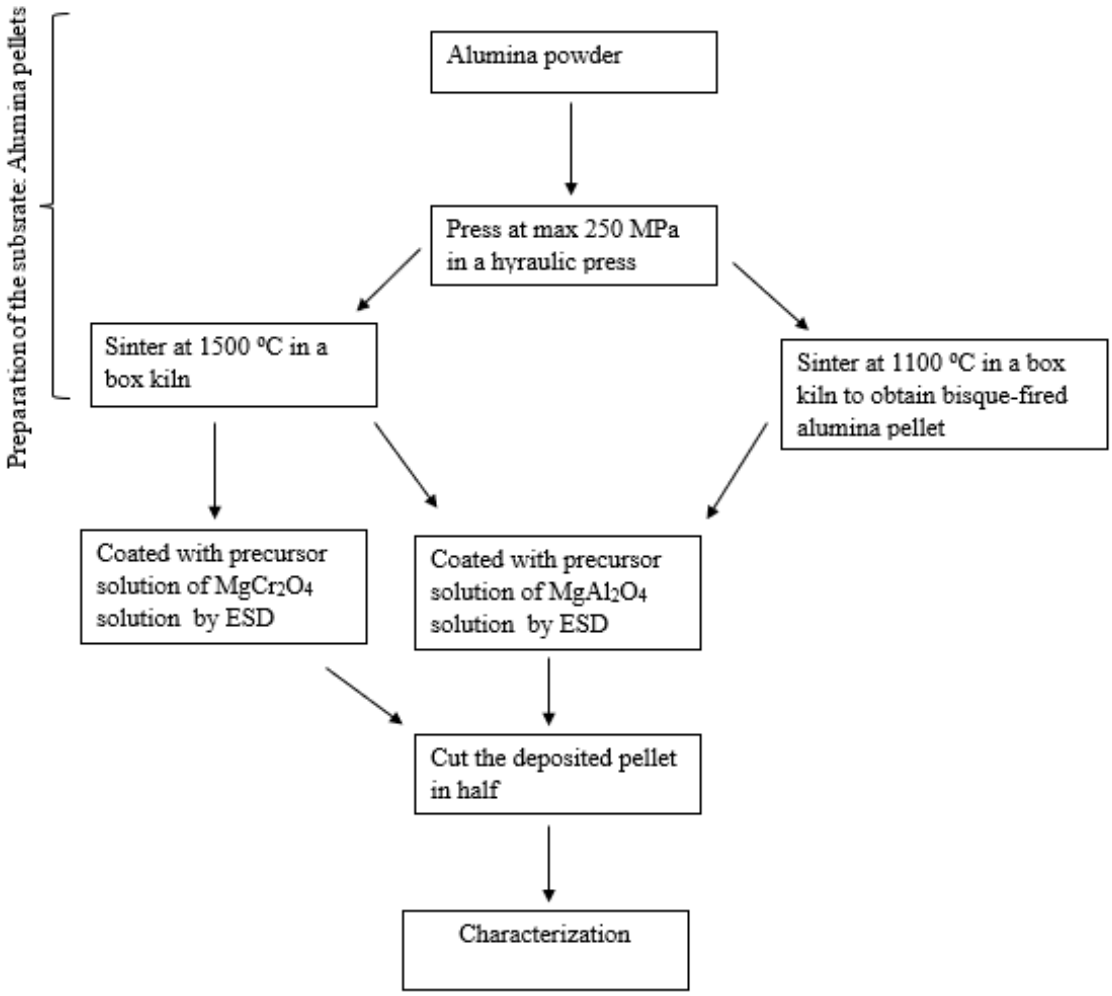

Figure 3.3. Flowchart of the experimental work followed in this thesis.

3.3. Characterization Analysis: XRD, SEM and EDX

Precursor solutions were characterized by energy dispersive X-ray spectroscopy methods (EDX) for elemental analysis.Both unheated and post heated precursor solutions were examined by X-ray diffraction (XRD, Panalytical X-Pert Pro).Analysis of coated pellets were performed by scanning electron microscopy (SEM-EDS, Philips XL 30S FEG).

3.3.1. Preparation of Precursor Solutions for XRD and EDX Analysis

20 mL of each precursor solution was taken into a beaker and placed in the oven to evaporate the solvents in the solution. The powders remaining in the beaker were taken into tubes and these amorphous powders were prepared for XRD and EDX analyses.

The powders remaining in the beaker after evaporation are amorphous oxide powders. These powders were kept in the furnace and annealed at 900^{o}C, 1000^{o}C, 1100^{o}C and 1200 ^{o}C degrees for 1 hour with a heating rate of 10 ^{o}C/min in order for them to transform into crystalline form and obtain the spinel structure. After the annealing procedures, the samples were ready for XRD analysis. Table 3.5 shows each preparation for the desired analysis.

Table 3.5. Material list prepared for XRD an EDX analysis.

Material	**XRD**	**EDX**
Amorphous Mg-rich-$MgAl_2O_4$ powder	+	+
Mg-rich-$MgAl_2O_4$ powder annealed at 900^{o}C	+	+
Mg-rich-$MgAl_2O_4$ powder annealed at 1000^{o}C	+	+
Mg-rich-$MgAl_2O_4$ powder annealed at 1100^{o}C	+	+
Mg-rich-$MgAl_2O_4$ powder annealed at 1200^{o}C	+	+
Amorphous $MgAl_2O_4$ powder	+	+
$MgAl_2O_4$ powder annealed at 900^{o}C	+	+
$MgAl_2O_4$ powder annealed at 1000^{o}C	+	+
$MgAl_2O_4$ powder annealed at 1100^{o}C	+	+
$MgAl_2O_4$ powder annealed at 1200^{o}C	+	+
Amorphous $MgCr_2O_4$ powder	+	+
$MgCr_2O_4$ powder annealed at 900^{o}C	+	+
$MgCr_2O_4$ powder annealed at 1000^{o}C	+	+
$MgCr_2O_4$ powder annealed at 1100^{o}C	+	+
$MgCr_2O_4$ powder annealed at 1200^{o}C	+	+

3.3.2. Preparation of the Coated Pellets for SEM Analysis

For SEM analysis, the coated pellets were crushed by a light strike with a hammer and made ready for analysis. Coated pellets would have been cut using a diamond saw but that would have produced too many debris which would have jeopardized SEM observation. A simple fracture surface therefore provided a good view of the cross sectional image.

3.3.3. Characterization Analysis Plan

Characterization analysis plan followed in this thesis is illustrated in Figure 3.4.

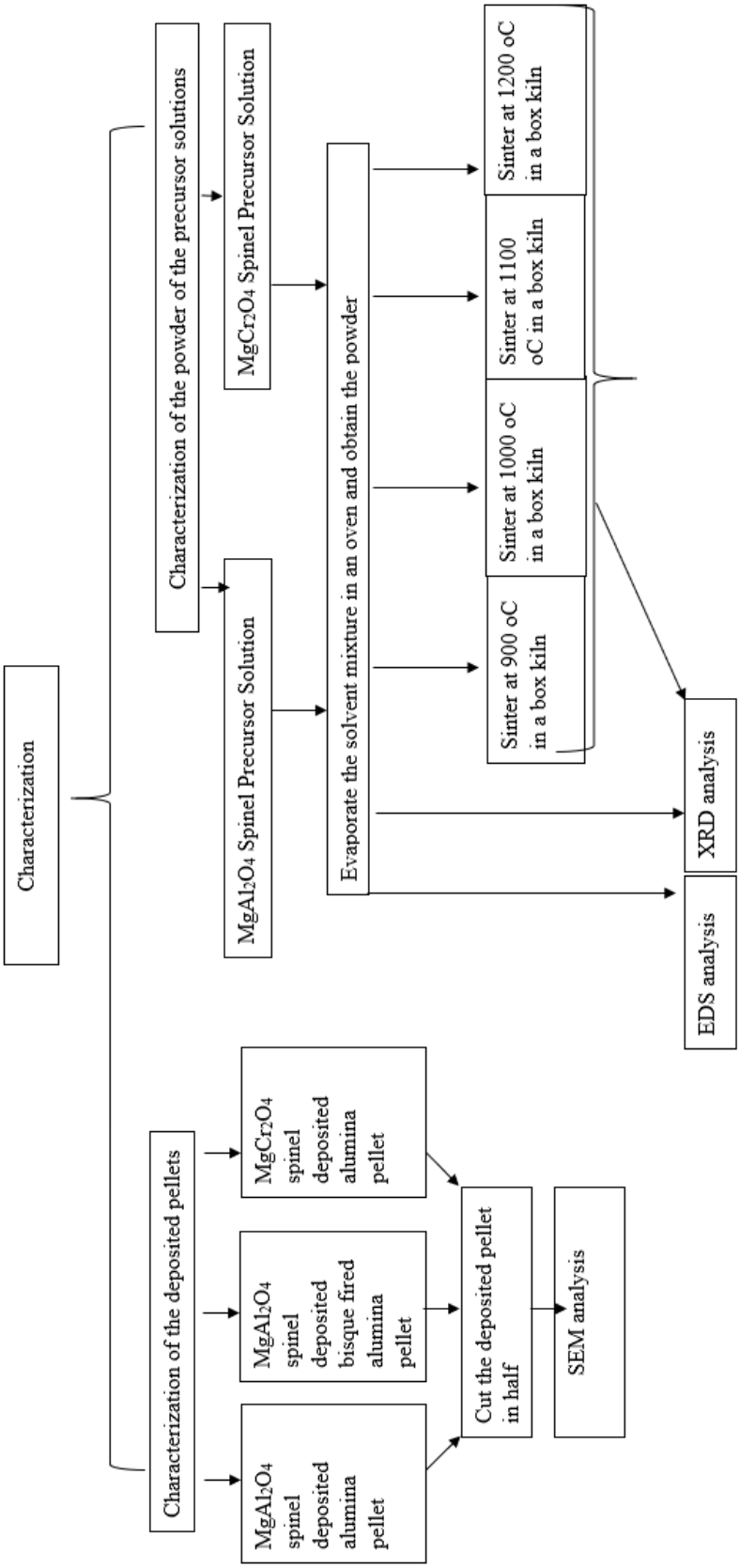

Figure 3.4. Flowchart of the characterization analysis followed in this thesis.

CHAPTER 4

RESULTS AND DISCUSSION

In this chapter, the results of the experiments in order to obtain the porous deposits of spinel structure on the alumina pellets and to determine the most influential parameter among the distance between needle and the substrate, the flow rate of the precursor solution and the applied voltage are presented and discussed. Besides, the optimum conditions which are given the best porous layer are determined.

In the first part, EDX analysis of the residue powders of the precursor solutions are presented. In the second part, SEM images of the coated pellets are discussed. In the third part, ANOVA table is given and the results are discussed. In the last part, the results of XRD analysis of both unheated and post heated powders of the precursor solutions are illustrated. The powders were heated at 900 ^{o}C, 1000 ^{o}C, 1100^{o}C and 1200^{o}C, respectively.

- **Spinel Coating on Alumina Pellet by Electrolytic Spray Depositon Method**

The alumina pellets were successfully coated with magnesium aluminate spinel layers by ESD method. Figure 4.1 shows a sample alumina pellet coated by magnesium aluminate spinel.

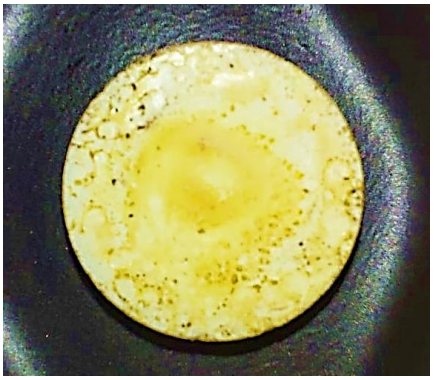

Figure 4.1. An example photograph of a $MgAl_2O_4$ spinel coated alumina pellet.

4.1. EDX Analysis

In this sub-section, EDX analysis of the residue powders of the precursor solutions are presented.

4.1.1. EDX Analysis of Mg-Rich $MgAl_2O_4$ Spinel Precursor Solution

Energy dispersive X-ray spectroscopy (EDX) analyses were performed in order to obtain the elemental content and percentage of the Mg-rich spinel precursor solution to be coated on the alumina substrates.

The solvent mixture of the solution was evaporated at around 200^oC in the oven as in the way which was explained in experimental section of this thesis, Chapter 3. Remaining powder was analyzed by EDS. The results are presented in Figure 4.2 and Table 4.1.

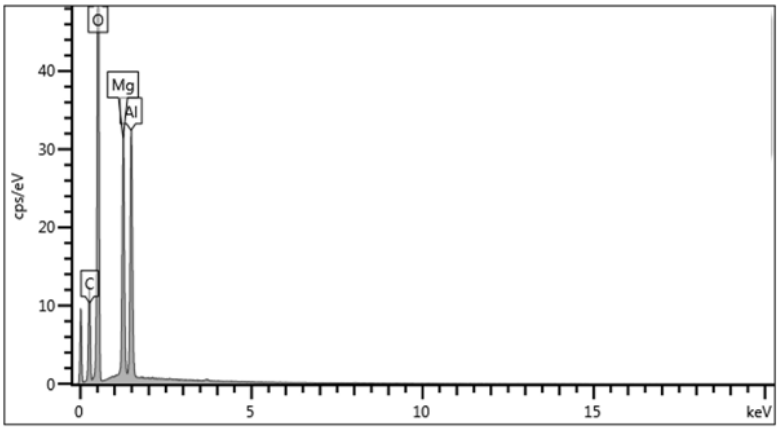

Figure 4.2. The result of EDX analysis of the remaining powder of Mg-rich $MgAl_2O_4$ spinel solution. Each element present in the solution is represented by the peaks in the graph.

Table 4.1. The weight and atomic percentages of the elements present in the remaining powder of Mg-rich $MgAl_2O_4$ spinel solution.

Element	**Weight %**	**Atomic %**	**Weight % in Spinel Stoichiometry**	**Atomic % in Spinel Stoichiometry**
C	22.97	31.01	-	-
O	53.14	53.87	44.98	57.14
Mg	11.42	7.62	17.09	14.29
Al	12.47	7.50	37.93	28.57
Total	100.00	100.00	100.00	100.00

In accordance with the EDX analysis of the solution, it can be said that the solution physically consisted of the atoms of Mg, Al and O which are necessary to be combined to form a magnesium aluminate spinel crystalline structure.

The prepared solution had excess of Mg elements which made the solution rich in terms of Mg elements. It can be said that the salt of $Mg(NO_3)_2$ dissolved in the solution faster.

Undesired C atoms were also presented. It is thought that these are the C atoms residue from the solvent mixture.

4.1.2. EDX Analysis of $MgAl_2O_4$ Spinel Precursor Solution

Energy dispersive X-ray spectroscopy (EDX) analyses was performed in order to obtain the elemental content and percentage of $MgAl_2O_4$ spinel precursor solution to be coated on the alumina substrate.

The residue powder was prepared in the same way as Mg-rich spinel solution. The result is presented in Figure 4.3 and Table 4.2 below.

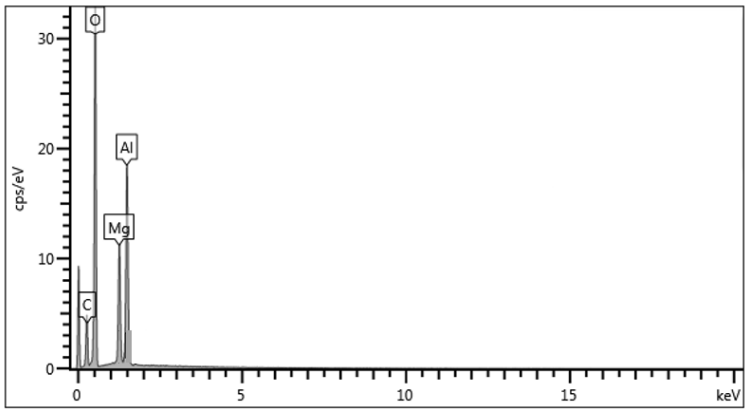

Figure 4.3. The result of EDX analysis of the remaining powder of $MgAl_2O_4$ spinel solution. Each element present in the solution is represented by the peaks in the graph.

Table 4.2. The weight and atomic percentages of the elements present in the remaining powder of $MgAl_2O_4$ spinel solution.

Element	**Weight %**	**Atomic %**	**Weight % in Spinel Stoichiometry**	**Atomic % in Spinel Stoichiometry**
C	19.25	25.67	-	-
O	55.57	57.02	44.98	57.14
Mg	8.86	5.99	17.09	14.29
Al	16.32	11.32	37.93	28.57
Total:	100.00	100.00	100.00	100.00

In accordance with the EDX analysis of the solution, it can be said that the solution physically consisted of the atoms of Mg, Al and O which are necessary to be combined to form a magnesium aluminate spinel crystalline structure. It can be also said that the salt of $Mg(NO_3)_2$ dissolved in the solution faster.

Undesired C atoms were also presented. It is thought that these are the C atoms residue from the solvent mixture.

4.1.3. EDX Analysis of $MgCr_2O_4$ Spinel Precursor Solution

Energy dispersive X-ray spectroscopy (EDX) analyses were performed in order to obtain the elemental content and percentage of $MgCr_2O_4$ spinel precursor solution to be coated on the alumina substrate.

The residue powder was prepared in the same way as Mg-rich spinel solution. The result is presented in Figure 4.4 and Table 4.3 below.

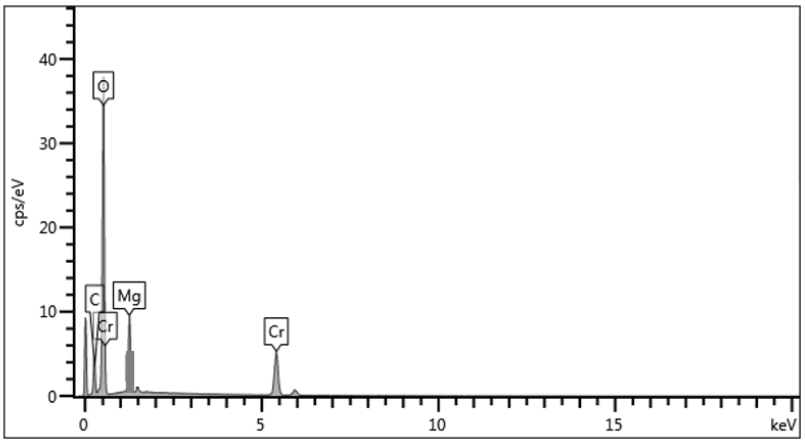

Figure 4.4. The result of EDX analysis of the remaining powder of $MgCr_2O_4$ spinel solution. Each element present in the solution is represented by the peaks in the graph.

Table 4.3. The weight and atomic percentages of the elements present in the remaining powder of $MgCr_2O_4$ spinel solution.

Element	**Weight %**	**Atomic %**	**Weight % in Spinel Stoichiometry**	**Atomic % in Spinel Stoichiometry**
C	8.42	19.65	-	-
O	51.92	61.20	44.98	57.14
Mg	9.18	7.12	17.09	14.29
Cr	30.48	12.03	37.93	28.57
Total:	100.00	100.00	100.00	100.00

In accordance with the EDX analysis of the solution, it can be said that the solution physically consisted of the atoms of Mg, Cr and O which are necessary to be combined to form a magnesium chromate spinel crystalline structure. It can be also said that the salt of $Mg(NO_3)_2$ dissolved in the solution faster.

Undesired C atoms were also presented. It is thought that these are the C atoms residue from the solvent mixture.

4.2. SEM Analysis

In this sub-section, SEM analysis of spinel deposited alumina pellets are presented.

4.2.1. SEM Images of the Alumina Pellets Deposited by Spinel Precursor Solution

The SEM images of the alumina pellets which were deposited by ESD varying the experimental conditions (Table 3.4) are presented. Both surface morphologies and cross sectional views of the coated pellets are shown.

4.2.1.1 SEM Images of Morphologies of Mg-Rich Spinel Deposited Alumina Pellets

The SEM images of the dense alumina pellets (sintered at 1500 ^{o}C) which were deposited by ESD varying the experimental conditions are presented in Figure 4.5 and Figure 4.9. As it is also stated in Chapter 3 of this study, 0.025 M of Mg rich magnesium aluminate spinel precursor solution was coated during 10 min. The deposition temperature was controlled at 300 ^{o}C.

Before starting the experiments, the most suitable parameters were searched by testing some values of the parameters which were decided to be varied. The aim of these trials were to be able to form spinel layers adhered to the dense alumina surface. As it is stated in Chapter 3 of this thesis, those parameters are flow rate of precursor solution, applied voltage and nozzle to subsrate distance.

Throughout the trials, it was observed that these parameters were affected by each other and caused to destruction of the desired condition which would create a deposition. The correlation of these parameters were an essential factor. For example, flow rates less than 0.10 mL/h could not form any coating on the pellets with lower voltages than 6 kV. Voltages more than 10 kV caused changes in spraying mode and the convenient spraying mode was not observed. Therefore, voltages of 6 kV and 10 kV were decided to be studied. The desired spraying mode was Taylor cone jet. It was also realised that the desired condition which would form a deposition on the pellet was destroyed by the higher voltages if flow rate was higher than 0.25 mL/h. The distances more than 25 mm was not enough at decreasing flow rates. That is why, 0.10 mL/h and 0.25 mL/h of flow rates and 15 mm and 25 mm of working distances were chosen to be studied.

After the trials, the lower and the upper values of the parameters which could enable to create a layer were determined and decided to use in the experiments.

The optimum conditions for successful porous spinel microstructure of deposited layer on the alumina pellets were investigated by changing the decided values of the parameters during the experiments.

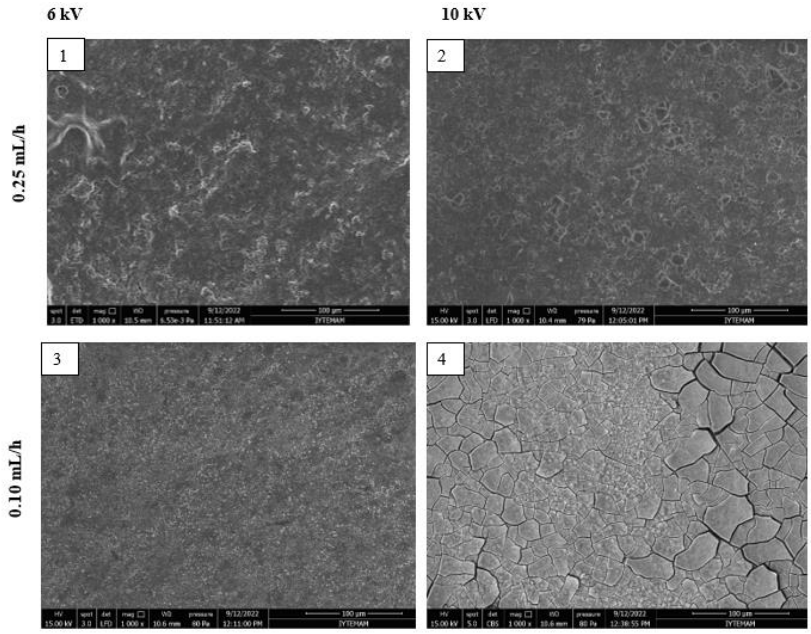

Figure 4.5. Surface morphologies of Mg rich $MgAl_2O_4$ spinel deposited alumina pellets.The distances between the nozzle tips and the pellets were 15 mm. Applied voltage of Sample 1 and 3 is 6 kV and 10 kV for Sample 2 and 4. Flow rates of the precursor solutions of Sample 3 and 4 is 0.10 mL/h and 0.25 mL/h for Sample 1 and 2.

In accordance with Figure 4.5, it was observed that a coral like deposition with porosities was developed on the surface of Sample 1 as seen on the cross sectional view in Figure 4.6. The reason of the development of this structure can be the successful access of the droplets to the hot surface of the alumina pellet to coat the surface homogeneously without causing any large gaps and cracks [37].

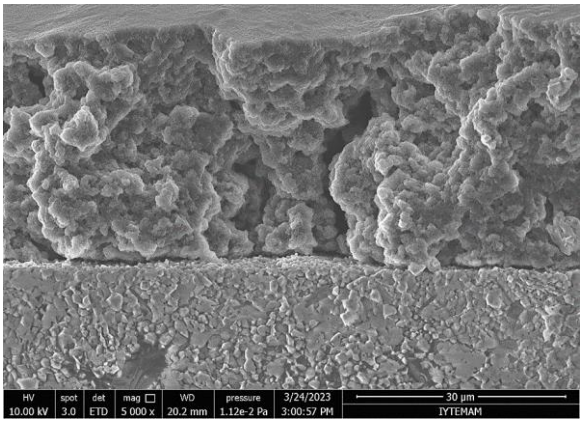

Figure 4.6. SEM image of the cross sectional morphology of Sample 1.

However, increasing the applied voltage from 6 kV to 10 kV brough about the cracks. Sample 2 possesses agglomerated particles with cracks. Figure 4.7 illustrates the cross sectional morphology of Sample 2. It has a relatively porous structure.

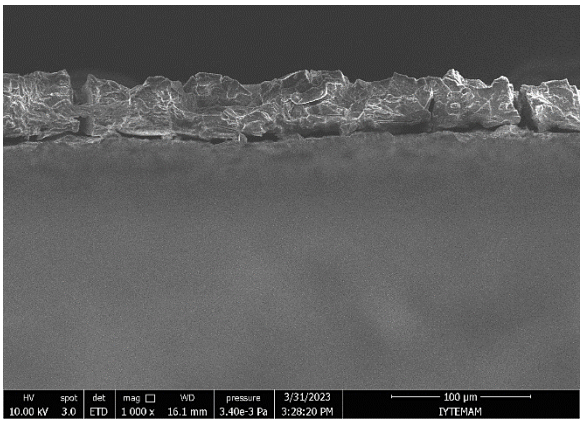

Figure 4.7. SEM image of the cross sectional morphology of Sample 2.

Sample 3 was observed to have dense and continuous structure with scattered small particles and pores (Figure 4.8). It was free of cracks.

It was clearly seen that Sample 4 had non-homogeneously scattered smaller particles formed on its surface compared to Sample 2. Figure 4.9 shows the cross sectional view of Sample 4. It had a good porous structure in accordance with this image.

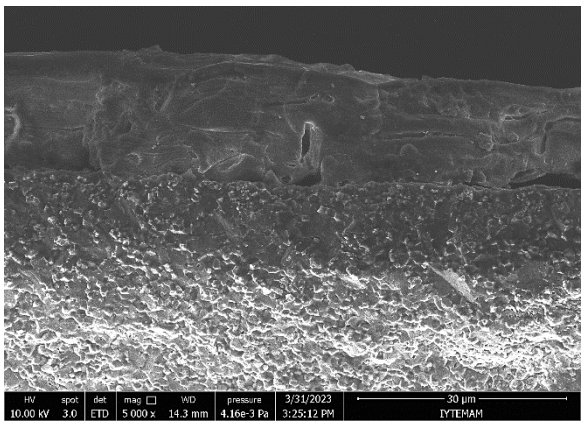

Figure 4.8. SEM image of the cross sectional view of Sample 3.

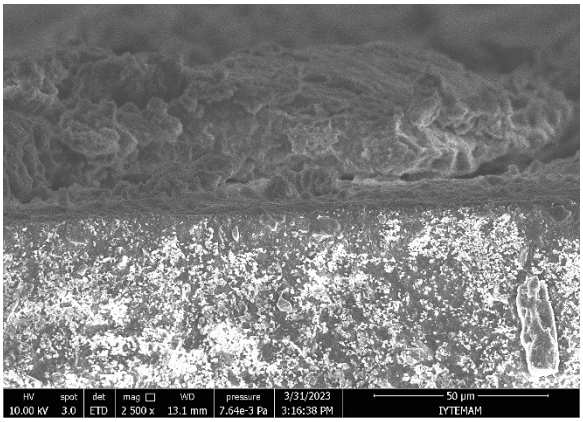

Figure 4.9. SEM image of the cross sectional view of Sample 4.

Figure 4.10 shows that the deposited layers tend to have a dense and cracked structure when the nozzle to subsrate distance is increased from 15 mm to 25 mm. While sample 6 owns a quite dense structure with macro-cracks, samples 5, 7 and 8 reveals a cracked structure with small particles on their surface. The reason of these layers is assumed to be influence of the working distance at high voltage. Increasing of working distance from 15 mm to 25 mm with the applied voltage of 10 kV cause a longer tranportation pathway. During the flight of the precursor solution from nozzle to the subsrate surface, solvent couple was evaporated prematurely. Thus, solidification of the particles occurred. Solidification caused to overlapping of the particles on the surface of the layer, which this is also called prefential landing in the literature [37].

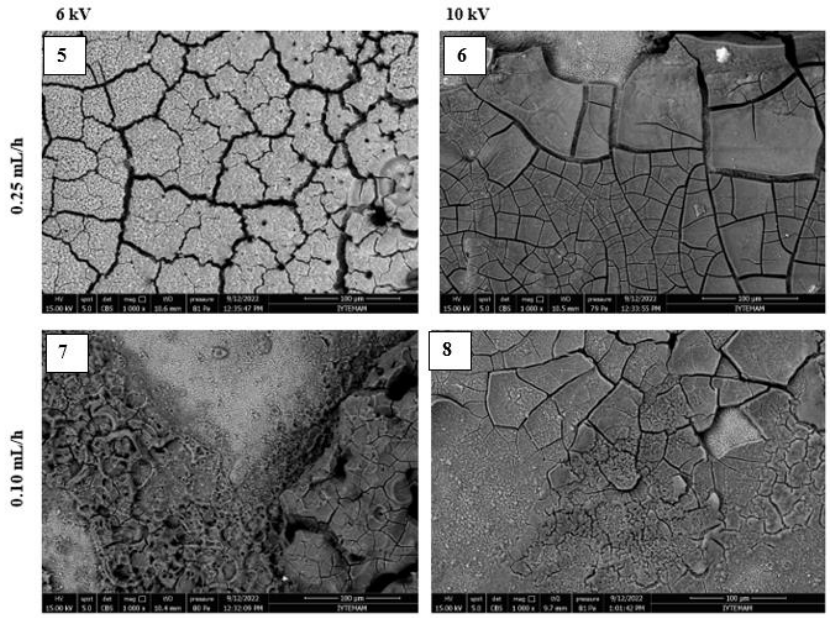

Figure 4.10. Surface morphologies of Mg rich $MgAl_2O_4$ spinel deposited alumina pellets.The distances between the nozzle tips and the pellets were 25 mm. Applied voltage of Sample 5 and 7 is 6 kV and 10 kV for Sample 6 and 8. Flow rates of the precursor solutions of Sample 7 and 8 is 0.10 mL/h and 0.25 mL/h for Sample 5 and 6.

A reticulated structure with non-homogeneously dispersed and segregated particles was observed on the surface of Sample 7. It also had small porosities between those segragated areas. Figure 4.11 shows the cross sectional view of Sample 7.

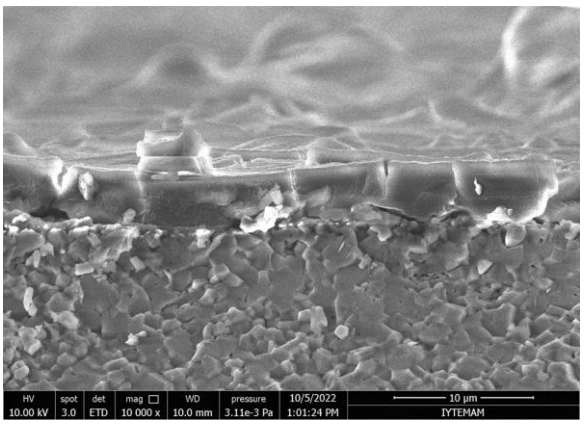

Figure 4.11. SEM image of the cross sectional view of Sample 7.

While Sample 6 had large and dense cracks, it was seen that Sample 8 had the same dense and cracked structure. Figure 4.12 reveals the cross sectional view of Sample 6.

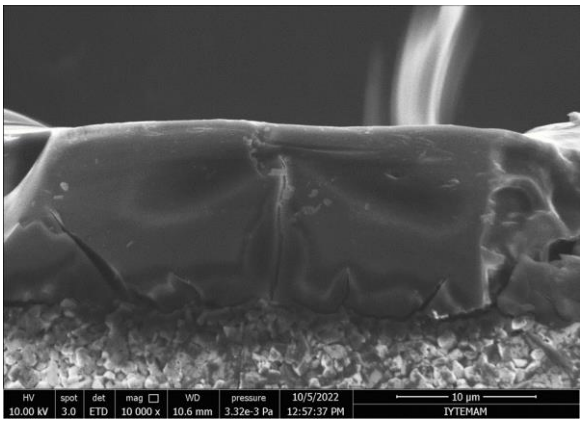

Figure 4.12. SEM image of the cross sectional view of Sample 6.

The coatings of Sample 4, 6 and 8 did not show strong adherence on the surface of the alumina pellets.

Sample 5 had cracks between a porous structure as shown in Figure 4.13.

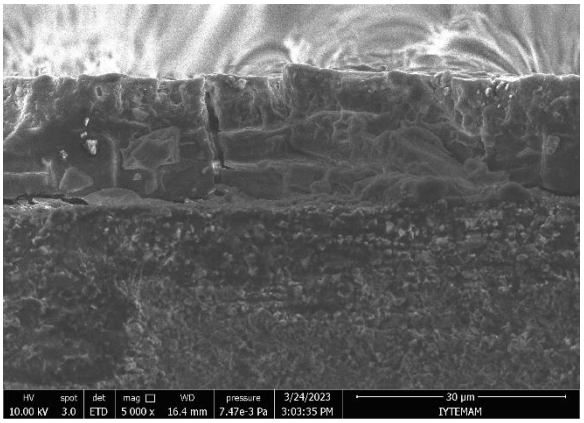

Figure 4.13. SEM image of cross sectional morphology of Sample 5.

Thanks to ESD method, many different coating structures were obtained by varying the parameters. The optimum conditions which gave a porous and coral like structure were selected as working distance of 15 mm, flow rate of 0.25 mL/h and applied voltage of 6 kV.

4.2.1.2. SEM Images of Morphologies of $MgAl_2O_4$ Spinel Deposited Alumina Pellet

$MgAl_2O_4$ spinel was deposited on the dense alumina pellet with the optimum conditions selected. The other parameters such as molarity of the precursor solution, the substrate temperature and the deposition time were kept the same as stated in the experimental section of this study. Figure 4.14 illustrates that a good porous and coral like structure was obtained and it was seen that this stoichometric difference between two solutions (Mg rich $MgAl_2O_4$ and $MgAl_2O_4$) was not a factor affecting the deposited layer.

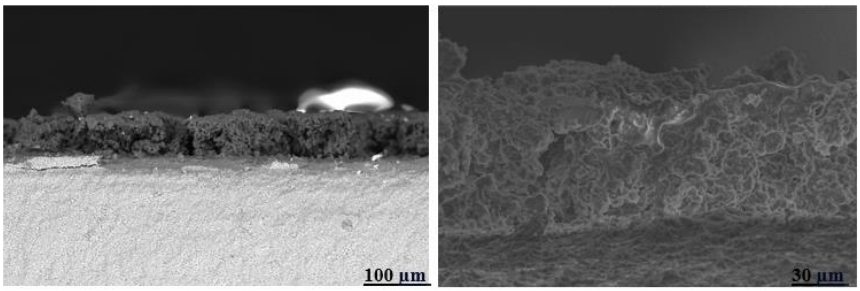

Figure 4.14. Cross sectional morphology of $MgAl_2O_4$ spinel deposited alumina pellet (sintered at 1500 ^oC). The sample was coated with a flow rate of 0.25 mL/h and the applied voltage of 6 kV. The distance beetween the nozzle tip and the pellet was 15 mm.

4.2.1.3. SEM Images of Morphologies of $MgAl_2O_4$ Spinel Deposited Bisque-Fired Alumina Pellet

$MgAl_2O_4$ spinel was deposited on the bisque- fired alumina pellet with the optimum conditions selected. The other parameters such as molarity of the precursor solution, the subsrate temperature and the deposition time were kept the same as stated in the experimental section of this study. Bisque-firing was done in order to see if the coating intruded pores in alumina. Figure 4.15 reveals that a good porous and coral like structure was obtained and it was seen that the substrate structure did not affect the

deposited layer. Moreover, it was observed that because bisque-fired pellet had more porous structure, the coating adhered well on the surface of the alumina pellet.

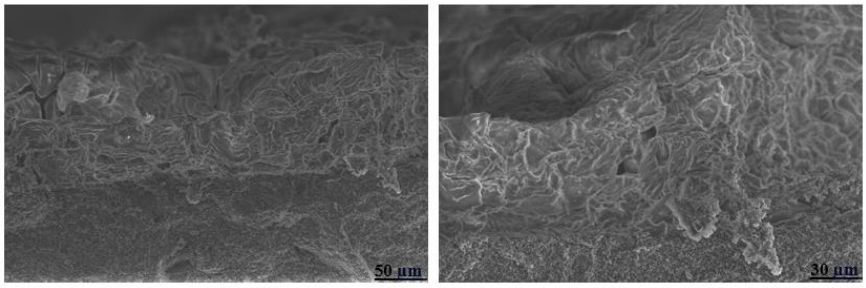

Figure 4.15. Cross sectional morphology of $MgAl_2O_4$ spinel deposited bisque-fired alumina pellet (sintered at 1100 ^oC). The sample was coated with a flow rate of 0.25 mL/h and the applied voltage of 6 kV. The distance beetween the nozzle tip and the pellet was 15 mm.

4.2.1.4. SEM Images of Morphologies of $MgCr_2O_4$ Spinel Deposited Alumina Pellet

In order to observe the diffusion of chromium into the alumina pellet, $MgCr_2O_4$ spinel was deposited on the dense alumina pellet by using the optimum conditions and the other parameters were the same as stated in Chapter 3 of this study.

Chromium was used as a marker, because Cr is heavier, hence brighter in SEM. Due to insufficient dissolution of $Cr(NO_3)_3$ in the solution, Cr was not clearly bright in SEM images.

Figure 4.16 shows the photograph of $MgCr_2O_4$ spinel layer on the alumina pellet after the deposition. It was surprisingly observed that the deposited layer was quite dense without any porosity as illustrated in Figure 4.17.

Figure 4.16. The photograph of $MgCr_2O_4$ spinel coated alumina pellet.

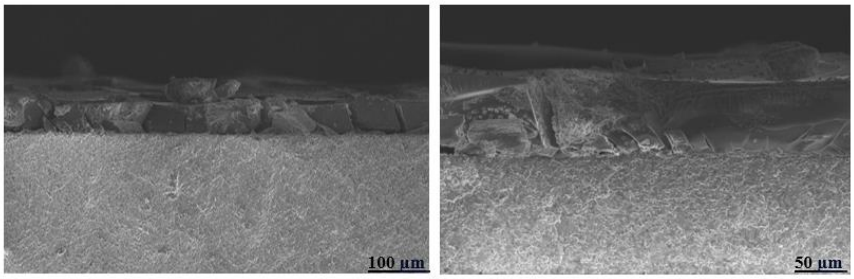

Figure 4.17. Cross sectional morphology of $MgCr_2O_4$ spinel deposited alumina pellet (sintered at 1500 ^oC). The sample was coated with a flow rate of 0.25 mL/h and the applied voltage of 6 kV. The distance between the nozzle tip and the pellet was 15 mm.

4.3. Statistical Analysis

Each of the alumina pellets coated using the ESD set-up and designing the experiments in accordance with the full factorial experimental design method were scored as in Table 4.4 according to the degree of porosity of the coating.

Table 4.4. Scores for an obtained porous structure.

Score / **Sample Code**	**Porous Structure**
1	5
2	4
3	3
4	5
5	3
6	1
7	1
8	1

Table 4.5 reveals the ANOVA table obtained from trial version of Minitab Software [53]. Independent variables were analysed one by one in order to investigate their effect on forming a porous layer on the alumina substrates. ANOVA analysis shows that working distance is significant parameter on being obtained a porous layer on the alumina pellets because it was seen that its P value was less than 0.10 as stated in the literature [51].

Table 4.5. Analysis of variance (ANOVA) table [53] .

Source	**DF**	**Adj SS**	**Adj MS**	**F-value**	**P-value**
Model	3	163.75	54.58	4.85	0.081
Linear	3	163.75	54.58	4.85	0.081
Working distance (mm)	1	151.25	151.25	13.44	**0.021**
Flow rate (mL/h)	1	11.25	11.25	1.00	0.374
Applied voltage (kV)	1	0.13	0.13	0.11	0.756
Error	4	45.00	11.25		
Total	7	208.75			

4.4. XRD Patterns of Unheated and Post-heated Powders of the Precursor Solutions

The crystal structures of the remaining powders of the precursor solutions after the evaporation was investigated by X-ray diffraction (XRD) analysis.

Coatings on alumina pellets were obtained by using 3 different precursor solutions (Mg rich $MgAl_2O_4$ spinel, $MgAl_2O_4$ spinel and $MgCr_2O_4$ spinel solutions) by ESD set-up. Since it was aimed to form spinel coatings on alumina pellets by ESD method in this thesis, XRD analyzes were performed to examine the structure of depositions on the pellets and to find out at what temperature a spinel structure can be obtained after post-heating and if the deposited layer is amorphous, or not.

It had been assumed that the obtained layers on the alumina pellets were amorphous structures because of the deposition at 300 ^oC and post-heating was required for the obtained coatings to turn into spinel structures. However, since the depositions on the pellets were insufficient for XRD analysis, it was performed on residuals of precursor solutions.

For this purpose, each residual powder from each precursor solution (Mg rich $MgAl_2O_4$ spinel, $MgAl_2O_4$ spinel and $MgCr_2O_4$ spinel solutions) was divided into five parts. One of these parts were remained unheated and the rest was post-heated in the furnace at 900^oC, 1000^oC, 1100^oC and 1200 ^oC for 1 hour with a heating rate of 10 ^oC/min as mentioned in Chapter 3 of this thesis. Figure 4.18, 4.19 and Figure 4.20 demostrate the formed structures of unheated and post-heated powders.

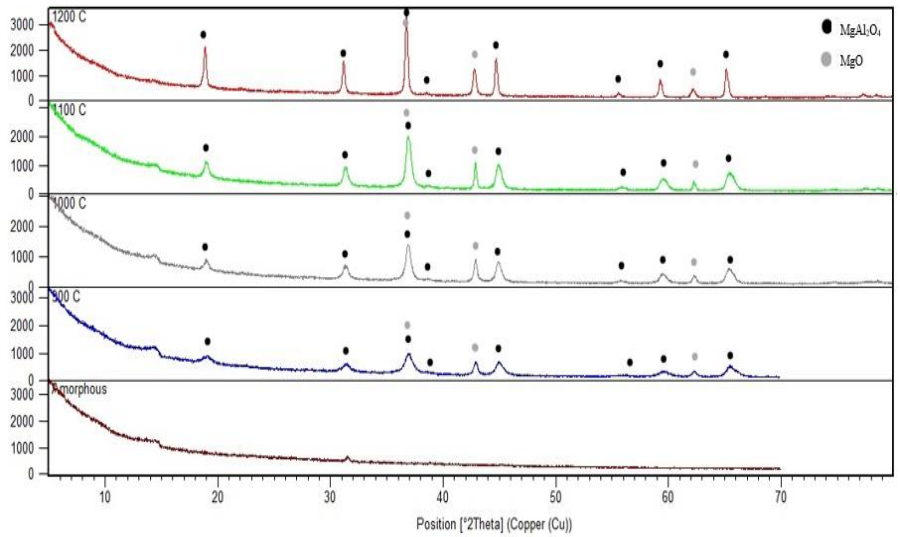

Figure 4.18. XRD pattern for Mg-rich $MgAl_2O_4$ spinel precursor solution residue after evaporation. The residues were heated at 900, 1000, 1100 and 1200 ^oC for 1 h before XRD measurements. JCPDS card numbers for the observed phases are: 01-082-2424 for $MgAl_2O_4$,00-045-0946 for MgO.

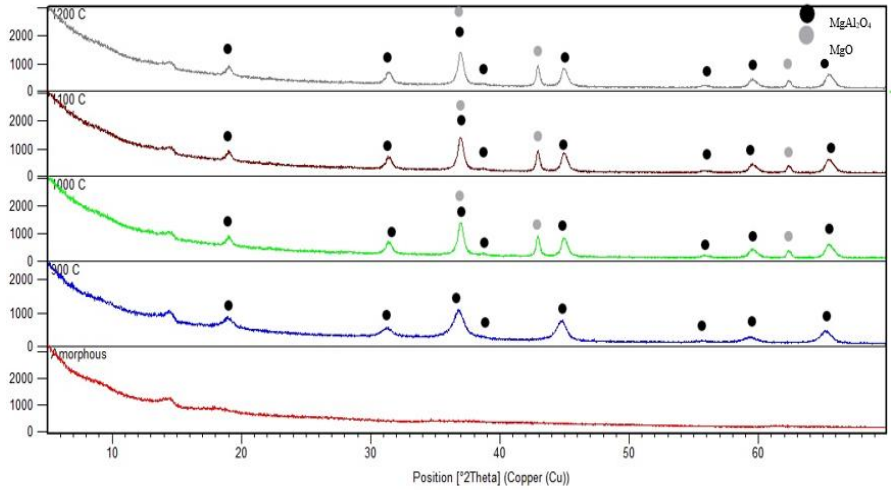

Figure 4.19. XRD pattern for $MgAl_2O_4$ spinel precursor solution residue after evaporation. The residues were heated at 900, 1000, 1100 and 1200 ^oC for 1 h before XRD measurements. JCPDS card numbers for the observed phases are: 01-082-2424 for $MgAl_2O_4$, 00-045-0946 for MgO.

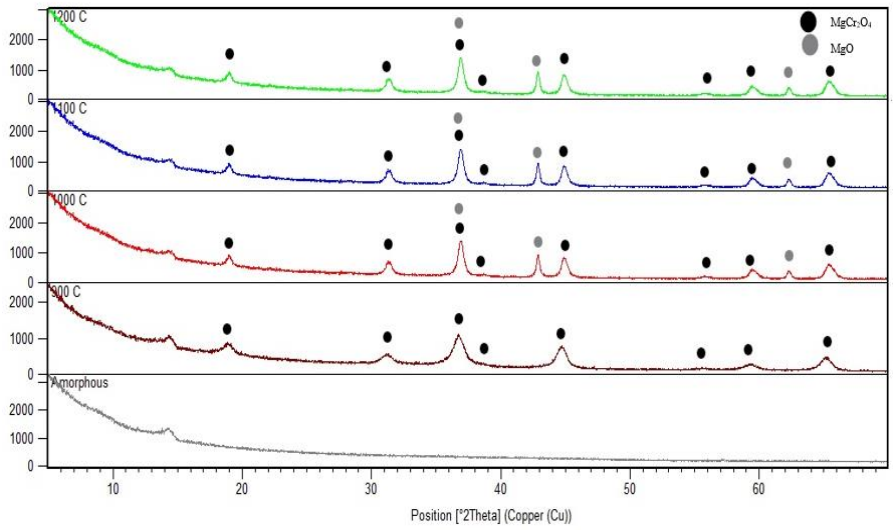

Figure 4.20. XRD pattern for $MgCr_2O_4$ spinel precursor solution residue after evaporation. The residues were heated at 900, 1000, 1100 and 1200 ^oC for 1 h before XRD measurements. JCPDS card numbers for the observed phases are: 00-010-0351 for $MgCr_2O_4$, 00-045-0946 for MgO.

XRD analysis has proved that the deposited layers on alumina pellets were amorphous before heating in the furnace. There was no peak indicating the presence of spinel structure. Nevertheless, the peaks referring a spinel structure formed after heating the powders at 900^oC, 1000^oC, 1100^oC and 1200 ^oC in the furnace were observed in the XRD patterns. Besides, a secondary phase called periclase (MgO) was formed after heating. Formation of MgO can cause problems due to the thermal expansion coefficient mismatch. MgO has a quite larger thermal expansion coefficient than $MgAl_2O_4$ and $MgCr_2O_4$ spinels. As a result, the coating can crack during heating/cooling cycles due to this reason.

The periclase phase should have been reacted with amorphous alumina in order to form $MgAl_2O_4$ spinel structure and with amorphous chromium oxide (Cr_2O_3) to form $MgCr_2O_4$ spinel. Another way of eliminating periclase is to prevent its formation. In order to achieve this, the stoichiometry of $Mg(NO_3)_2$ in the solution can be arranged accordingly. Due to the fact that $Mg(NO_3)_2$ dissolved well in the solution compared to the other nitrate salts: $Al(NO_3)_3$ and $Cr(NO_3)_3$. The solution was poor in terms of Al^{3+} and Cr^{3+} ions. That is why, periclase formation was observed.

In accordance with the XRD peaks obtained, it can also be said that as the heating temperatures of the powders was increased, sharper and longer peaks were observed.

Apart from that, the widths of the resulting peaks show the size of the crystal structure formed. It can be reported that the resulting structure has nano-sized particles.

CHAPTER 5

CONCLUSION

This thesis presents for the first time in the literature, to the best of my knowledge, an experimental study of deposition of spinel layers on dense alumina pellets by electrostatic spray deposition technique.

In this work, the main goals were to deposit spinel layer on dense alumina pellet by ESD. As the ESD process depends on a number of processing variables, the number of experiments required to fully understand the effect of each variable on the resulting coating structure was prohibitive, hence statistical experimental design methods were used to minimize the number of experimental runs to obtain valid conclusions. A full factorial experimental design method was employed with 8 experimental runs. The purpose was to search for the best process parameters to obtain a porous layer and to investigate the results of varying ESD process parameters (working distance, applied voltage and flow rate of the sprayed solution) on the coating structure obtained.

$MgAl_2O_4$ spinel layers were successfully coated on the dense alumina pellets by using ESD method which is a low-cost, easy to operate and versatile when compared to other deposition techniques.

EDX results of precursor solutions showed that desired elements to form spinel structure were sprayed onto the alumina pellets.

The results of SEM analysis revealed that ESD technique enables to attain several kind of deposited microstructures on alumina pellets. Changes in nozzle to substrate distance, applied voltage and flow rate of the spraying solution, that were the main ESD process parameters, were found to play an important role on the resulting layer. The most suitable conditions for a porous layer were working distance of 15 mm, flow rate of 0.25 mL/h and applied voltage of 6 kV in this study. Relatively high working distance at high voltage resulted in preferential landing which is explained in the literature as solidification of the coating particles during the transportation and overlapping of the

layers on the alumina pellets, consequently. The obtained ANOVA table revealed that the most significant and effective parameter varying the structure of the deposited layer was working distance in this experimental work.

XRD analysis proved that the layers coated on the alumina pellets before further heating were amorphous. Upon heating, crystalline spinel layers on alumina substrates were able to be obtained. Spinel phase appeared in the XRD pattern after heating at 900^{o}C, 1000^{o}C, 1100^{o}C and 1200 ^{o}C. There was also another phase called periclase showed up on the coating layers accordingly XRD results. This phase probably formed as a result of insufficient dissolution of Al bearing precursor solution. Due to the formation of periclase phase, the thermal expansion coefficient mismatch of MgO and $MgAl_2O_4$ and $MgCr_2O_4$ spinels would result in problems. MgO has larger thermal expansion coefficient than $MgAl_2O_4$ and $MgCr_2O_4$ spinels. As a result, the coating can crack during heating/cooling cycles.

It is concluded that there are varied coating methods with their advantages and disadvantages mentioned in the literature. In this thesis, deposition of spinel layer on alumina was studied for the first time. The deposition parameters were investigated in an empirical approach.

This study can be improved in order to investigate the effects of ESD process parameters further and to vary the deposited microstructures.

In order to prevent MgO formation, a balance stoichiometry of the precursor solution can be achieved by using better dissolving Al bearing precursor solution in the ethanol and butlyl carbitol mixtures. Different solute mixtures, which are able to dissolve $Al(NO_3)_3$ and $Cr(NO_3)_3$ better, can be also searched in the further studies.

The layers were obtained on the alumina pellets at the deposition temperature of 300 ^{o}C. Post-heating is required for the obtained coatings to turn into crystalline spinel structures and to be able to observe the possible diffusive interaction between the spinel coating and the alumina substrate.

REFERENCES

[1] W. Callister and D. Rethwisch, *Materials science and engineering: An introduction*. John Wiley & Sons, Inc., 2010.

[2] Pertti. Auerkari, *Mechanical and physical properties of engineering alumina ceramics*. Technical Research Centre of Finland, 1996.

[3] Y. Palacı, "Alüminanın özelliklerine, şekillendirme yönteminin, katkıların ve sinterleme sıcaklığının etkisi", İstanbul, Turkey: İstanbul Technical University, 2001.

[4] M. G. Baronskiy, S. v. Tsybulya, A. I. Kostyukov, A. v. Zhuzhgov, and V. N. Snytnikov, "Structural properties investigation of different alumina polymorphs (η-, γ-, χ-, θ-, α-Al2O3) using Cr3+ as a luminescent probe," *J Lumin*, vol. 242, Feb. 2022, doi: 10.1016/j.jlumin.2021.118554.

[5]https://chem.libretexts.org/Bookshelves/Inorganic_Chemistry/Book%3A_Introduction_to_Inorganic_Chemistry_(Wikibook)/08%3A_Ionic_and_Covalent_Solids_-_Structures/8.07%3A_Spinel_Perovskite_and_Rutile_Structures#:~:text=The%20spinel%20structure%20is%20formulated,formula%20AB2O4. (18.02.2023, 08:32)

[6] S. Hashimoto, S. Honda, T. Hiramatsu, and Y. Iwamoto, "Fabrication of porous spinel (MgAl2O4) from porous alumina using a template method," *Ceram Int*, vol. 39, no. 2, pp. 2077–2081, Mar. 2013, doi: 10.1016/j.ceramint.2012.08.062.

[7] A. Shafeiey, M. H. Enayati, and A. Al-Haji, "The effect of slip casting parameters on the green density of MgAl2O4 spinel," *Ceram Int*, vol. 43, no. 8, pp. 6069–6074, Jun. 2017, doi: 10.1016/j.ceramint.2017.01.151.

[8] https://www.sciencedirect.com/topics/chemistry/solid-state-reaction. (02.02.2023, 21:43)

[9] R. Garg *et al.*, "Plasma CVD grown Al2O3 and MgAl2O4 coatings for corrosion protection applications," *Surf Coat Technol*, vol. 356, pp. 49–55, Dec. 2018, doi: 10.1016/j.surfcoat.2018.09.054.

[10] D. Beckel *et al.*, "Thin films for micro solid oxide fuel cells," *J Power Sources*, vol. 173, no. 1, pp. 325–345, Nov. 2007, doi: 10.1016/j.jpowsour.2007.04.070.

[11] A. Princiville and E. Djurado, "Nanocomposıte Cathode For SOFCs Prepared by Electrostatıc Spray Deposıtıon," World Scientific Pub Co Pte Lt, Jun. 2006, pp. 305–312. doi: 10.1142/9789812773104_0035.

[12] E. Yalamac, C. Carry, and S. Akkurt, "Microstructural development of interface layers between co-sintered alumina and spinel compacts," *J Eur Ceram Soc*, vol. 31, no. 9, pp. 1649–1659, Aug. 2011, doi: 10.1016/j.jeurceramsoc.2011.03.020.

[13] C. Durucan, A. Öztürk, M. Timuçin, “Ceramıc Materıals Met E 451”, Ankara, Turkey: METU, Metallurgical and Materials Engineering Department, 2009.

[14] E.Yalamaç,“Sınterıng, Co-sınterıng and Mıcrostructure Control of Oxıde Based Materıals : Zırconıa, alumına, spınel, alumına-zırconıa and spınel-alumına,” İzmir, Turkey: Iztech, Mechanical Engineering Department, 2010.

[15] “https://ceramics.org/about/what-are-engineered-ceramics-and-glass/structure-and-properties-of-ceramics.” (17.10.2022, 11:30)

[16] J. George, D. Waroquiers, D. di Stefano, G. Petretto, G. Rignanese, and G. Hautier, “The Limited Predictive Power of the Pauling Rules,” *Angewandte Chemie International Edition*, vol. 59, no. 19, pp. 7569–7575, May 2020, doi: 10.1002/anie.202000829.

[17] https://www.chemistryscl.com/material-science/ceramics-crystal-structure-characteristics-imperfections-applications/index.php. (19.01.2023, 22:17)

[18] B. Umroh, A. Ginting, and M. N. A. Rahman, “CO_2laser machining on alumina ceramic: A review,” in *IOP Conference Series: Materials Science and Engineering*, IOP Publishing Ltd, Dec. 2020. doi: 10.1088/1757-899X/1003/1/012131.

[19] N. F. Ishak, N. A. Hashim, M. H. D. Othman, P. Monash, and F. M. Zuki, “Recent progress in the hydrophilic modification of alumina membranes for protein separation and purification,” *Ceramics International*, vol. 43, no. 1. Elsevier Ltd, pp. 915–925, Jan. 01, 2017. doi: 10.1016/j.ceramint.2016.10.044.

[20] B. Ramogayana, D. Santos-Carballal, K. P. Maenetja, N. H. de Leeuw, and P. E. Ngoepe, “Density Functional Theory Study of Ethylene Carbonate Adsorption on the (0001) Surface of Aluminum Oxide α-Al $_2$ O $_3$,” *ACS Omega*, vol. 6, no. 44, pp. 29577–29587, Nov. 2021, doi: 10.1021/acsomega.1c03771.

[21] “https://www.sciencedirect.com/topics/chemistry/alpha-aluminium-oxide.” (15.11.2022, 21:40)

[22] R. Maschio, B. Fabbri, and C. Fiori, Industrial applications of refractories containing magnesium aluminate spinel, Industrial Ceramics, vol. 8, pp. 121-126, 1988.

[23] I. M. Low, *Ceramic-Matrix Composites,Microstructure, Properties and Applications*. Woodhead, 2006.

[24] I. Ganesh, “A review on magnesium aluminate ($MgAl_2O_4$) spinel: Synthesis, processing and applications,” *International Materials Reviews*, vol. 58, no. 2. pp. 63–112, Feb. 2013. doi: 10.1179/1743280412Y.0000000001.

[25] R. Dal Maschio and B. Fabbri, “Scientific analysis of early European porcelain View project.” [Online]. Available: https://www.researchgate.net/publication/284418284

[26] S. Leo, C. Tallon, N. Stone, and G. v. Franks, “Near-Net-Shaping Methods for Ceramic Elements of (Body) Armor Systems,” *Journal of the American Ceramic Society*, vol. 97, no. 10, pp. 3013–3033, Oct. 2014, doi: 10.1111/jace.13192.

[27] R. Shi, M. Wood, T. W. Heo, B. C. Wood, and J. Ye, “Towards understanding particle rigid-body motion during solid-state sintering,” *J Eur Ceram Soc*, vol. 41, no. 16, pp. 211–231, Dec. 2021, doi: 10.1016/j.jeurceramsoc.2021.09.039.

[28] M. O. Mavukkandy, S. A. McBride, D. M. Warsinger, N. Dizge, S. W. Hasan, and H. A. Arafat, “Thin film deposition techniques for polymeric membranes– A review,” *J Memb Sci*, vol. 610, Sep. 2020, doi: 10.1016/j.memsci.2020.118258.

[29] S. Arshad Hussain, B. Dey, D. Bhattacharjee, and N. Mehta, “Unique supramolecular assembly through Langmuir e Blodgett (LB) technique”, doi: 10.1016/j.heliyon.2018.

[30] B. Fotovvati, N. Namdari, and A. Dehghanghadikolaei, “On coating techniques for surface protection: A review,” *Journal of Manufacturing and Materials Processing*, vol. 3, no. 1. MDPI Multidisciplinary Digital Publishing Institute, Mar. 01, 2019. doi: 10.3390/jmmp3010028.

[31] C. H. Chen, E. M. Kelder, M. J. G. Jak, and J. Schoonman, “Electrostatic spray deposition of thin layers of cathode materials for lithium battery”.

[32] R. Neagu, D. Perednis, A. Princivalle, and E. Djurado, “Zirconia coatings deposited by electrostatic spray deposition A chemical approach,” *Solid State Ion*, vol. 177, no. 17–18, pp. 1451–1460, Jul. 2006, doi: 10.1016/j.ssi.2006.07.027.

[33] R. Neagu, D. Perednis, A. Princivalle, and E. Djurado, “Influence of the process parameters on the ESD synthesis of thin film YSZ electrolytes,” *Solid State Ion*, vol. 177, no. 19-25 SPEC. ISS., pp. 1981–1984, Oct. 2006, doi: 10.1016/j.ssi.2006.05.052.

[34] A. Jaworek and A. T. Sobczyk, “Electrospraying route to nanotechnology: An overview,” *J Electrostat*, vol. 66, no. 3–4, pp. 197–219, Mar. 2008, doi: 10.1016/j.elstat.2007.10.001.

[35] D. Marinha, C. Rossignol, and E. Djurado, “Influence of electrospraying parameters on the microstructure of La0.6Sr0.4Co0.2F0.8O 3-δ films for SOFCs,” *J Solid State Chem*, vol. 182, no. 7, pp. 1742–1748, Jul. 2009, doi: 10.1016/j.jssc.2009.04.018.

[36] J. Kim, Y. Park, D. J. Sung, S. Moon, K. B. Lee, and S. I. Hong, “Preparation of thin film YSZ electrolyte by using electrostatic spray deposition,” *Int J Refract Metals Hard Mater*, vol. 27, no. 6, pp. 985–990, Nov. 2009, doi: 10.1016/j.ijrmhm.2009.07.001.

[37] C. Sındıraç and S. Akkurt, “Microstructural investigation of the effect of electrospraying parameters on LSCF films,” *Int J Hydrogen Energy*, vol. 45, no. 60, pp. 35139–35148, Dec. 2020, doi: 10.1016/j.ijhydene.2020.02.194.

[38] N. Stelzer and J. Schoonman, “Synthesis of Terbia-doped Yttria-Stabilized Zirconia thin films by Electrostatic Spray Deposition (ESD) Electrochemistry of fuel oxidation on SOFC anode View project LOCOBOT View project,” 1996. [Online]. Available: https://www.researchgate.net/publication/27345169

[39] N. Bharadishettar, U. Bhat K, and D. B. Panemangalore, “Coating technologies for copper based antimicrobial active surfaces: A perspective review,” *Metals*, vol. 11, no. 5. MDPI AG, May 01, 2021. doi: 10.3390/met11050711.

[40] S. Sabooni *et al.*, “Fundamentals of the adhesion of physical vapor deposited ZnMg-Zn bilayer coatings to steel substrates,” *Mater Des*, vol. 190, May 2020, doi: 10.1016/j.matdes.2020.108560.

[41] M. Ferrer, F. Vargas, and C. M. Moreno, “Thermal properties of zirconia-alumina coatings obtained by thermal spray flame,” in *Journal of Physics: Conference Series*, Institute of Physics Publishing, Nov. 2019. doi: 10.1088/1742-6596/1388/1/012006.

[42] L. Pin, F. Ansart, J. P. Bonino, Y. le Maoult, V. Vidal, and P. Lours, “Reinforced sol-gel thermal barrier coatings and their cyclic oxidation life,” *J Eur Ceram Soc*, vol. 33, no. 2, pp. 269–276, Feb. 2013, doi: 10.1016/j.jeurceramsoc.2012.07.037.

[43] E. Yalamaç, S. Akkurt, and M. Çiftçioğlu, “Low temperature synthesis of spinel powders by mechanical grinding,” in *Key Engineering Materials*, Trans Tech Publications Ltd, 2004, pp. 53–56. doi: 10.4028/www.scientific.net/kem.264-268.53.

[44] N. Jeong, J. G. Yeo, and K. S. Song, “Direct synthesis of 20-nm-thick MgAl2O4 spinel nanowires on an alumina substrate and their use as supports for size-controlled platinum nanoparticles,” *Mater Lett*, vol. 109, pp. 34–37, 2013, doi: 10.1016/j.matlet.2013.05.110.

[45] X. H. Chen, C. Xiao, and J. Li, “Preparation of mgal2o4-coated al2o3np and migration of ceramic nanoparticles during ultrasonic processing of aluminum matrix composites,” *Coatings*, vol. 10, no. 11, pp. 1–17, Nov. 2020, doi: 10.3390/coatings10111039.

[46] S. Nuclei, “2015; 18(2) 405 Innovative Coating Method of MgAl 2 O 4 or ZnAl 2 O 4 on α-Al.”

[47] C. Voigt, E. Jäckel, C. G. Aneziris, and J. Hubálková, “Spinel coating on alumina foam ceramics for aluminum filtration,” *Adv Eng Mater*, vol. 15, no. 12, pp. 1197–1205, Dec. 2013, doi: 10.1002/adem.201300111.

[48] D. Nordstokke and S. M. Colp, “Factorial Design,” in *Encyclopedia of Quality of Life and Well-Being Research*, Dordrecht: Springer Netherlands, 2014, pp. 2144–2145. doi: 10.1007/978-94-007-0753-5_982.

[49] D. C. Montgomery, “*Design and analysis of experiments”*, John Wiley & Sons, Inc., 2013.

[50]https://www.investopedia.com/terms/a/anova.asp#:~:text=Analysis%20of%20variance%2C%20or%20ANOVA,the%20dependent%20and%20independent%20variables. (10.02.2023, 23:24)

[51] R. G. Brereton, “ANOVA tables and statistical significance of models,” *J Chemom*, vol. 33, no. 3, p. e3019, Mar. 2019, doi: 10.1002/cem.3019.

[52]“ https://www.almatis.com/media/hamk2s0i/gp-rcp_024_ct3000ls_sg_0812.pdf.” (18.03.2023, 18:32)

[53] https://www.minitab.com/en-us/. (12.01.2023, 23:01)